# MODELING AND DEVELOPMENT OF A ROBUST VIBRATION SUPPRESSION CONTROL SYSTEM FOR PISTON-TYPE AIR COMPRESSORS

**BY**

**JANE FRANCES NALUBEGA**

**(BSc. Agro-Processing Engineering, BU)**

**19/U/GMEM/18803/PD**

**A DISSERTATION SUBMITTED TO THE DIRECTORATE OF RESEARCH AND GRADUATE TRAINING IN PARTIAL FULFILMENT OF THE REQUIREMENTS FOR THE AWARD OF THE DEGREE OF MASTER OF SCIENCE IN ADVANCED MANUFACTURING SYSTEMS ENGINEERING DEGREE OF KYAMBOGO UNIVERSITY**

**AUGUST 2025**

## DECLARATION

This dissertation is my original work and has never been presented for a degree in any other university.

Sign. …… Date. ……

Jane Frances Nalubega.

19/U/GMEM/18803/PD

## APPROVAL

We as university supervisors confirm the work done by the candidate under our supervision.

Sign. …… Date. ……

MAIN SUPERVISOR: Dr. Kangwagye Samuel

Sign. …… Date. ……

CO-SUPERVISOR: Dr. Maureen Ssempijja Nalubowa

## DEDICATION

I dedicate this work to my supervisors, Eng. Dr. Kangwagye Samuel and Dr. Maureen Ssempijja Nalubowa, whose encouragement carried me through to the finish. I also acknowledge the teamwork demonstrated by the Department of Mechanical and Production Engineering at Kyambogo University, whose tremendous support has kept this program running smoothly.

My heartfelt gratitude goes to all my classmates who contributed to the completion of this dissertation.

**ACKNOWLEDGEMENT**

I am immensely grateful to have completed this dissertation under the expert guidance of Dr. Kangwagye Samuel and Dr. Maureen Ssempijja, who introduced me to the field of control systems. Working with them has been an enriching and rewarding experience.

I also extend my appreciation to my employer, Engineer Ivan Masuba, and my colleagues for providing me with the opportunity to reach this stage. Lastly, my heartfelt thanks go to my family for their unwavering support throughout this journey.

## TABLE OF CONTENTS

## LIST OF FIGURES

## LIST OF TABLES

## ABSTRACT

Piston-type air compressors are susceptible to excessive vibrations arising from periodic disturbances, which compromise energy efficiency, induce mechanical wear, and shorten equipment lifespan. Conventional control approaches often lack the robustness required for real-time vibration suppression. This research focuses on the modelling and development of a Disturbance Observer-Based (DOB) control system to actively mitigate such vibrations. A comprehensive dynamic model of the compressor system was formulated, integrating both motor and mechanical dynamics. Based on this model, a DOB control algorithm was designed to estimate and compensate for external disturbances in real time. The control strategy was implemented and evaluated in MATLAB/Simulink through simulation studies under varying disturbance profiles. Simulation results indicated that the DOB-based controller significantly outperformed the traditional feedback control method. Specifically, the proposed controller achieved a 57% reduction in overshoot, decreased the settling time from 0.20 seconds to 0.08 seconds, and demonstrated superior disturbance rejection under both square wave and sinusoidal excitation signals. Additionally, it maintained accurate reference tracking and stable operation under load variability. These results validate the effectiveness of the proposed DOB-based control framework in enhancing the performance, reliability, and operational stability of piston-type air compressors. The developed methodology provides a viable foundation for further experimental validation and real-time industrial deployment.



**Keywords**: piston-type air compressor, vibration suppression, disturbance observer, dynamic modelling, MATLAB/Simulink, robust control, disturbance rejection.

# CHAPTER ONE: INTRODUCTION

## 1.1 Background to the Study

Nagrale, (2024) highlighted that compressed air plays a critical role in global industrial development, noting that over 70% of manufacturers utilize compressed air systems. Lu et al., (2023) also reported that these systems account for approximately 20% of electricity consumption. Bonfá et al., (2019) reported that a stable and efficient air compression system supports continuous operations. Nehler et al., (2018) stated that compressed air systems (CAS) are tailored to meet production requirements in processes such as assembling, clamping, cushioning, processing, and drying. Lu, Zhang, & Wang, (2023) noted that approximately 20% of industrial energy is consumed in compressed gas production, yet less than 30% of that energy is used efficiently.

Currently, Disturbance Observer-Based (DOB) control systems have gained popularity due to their ability to reduce the effects of unwanted disturbances in real time. Researchers noted that, unlike conventional feedback controllers that respond only after a disturbance impacts the system, DOB-based controllers could detect it in advance and counteract it before it harms performance. This capability makes them particularly suitable for systems subject to constant changes, such as piston-type air compressors. Das et al., (2023) demonstrated the effectiveness of DOB in reducing vibrations in rotating machines. Similarly, Park et al., (2024) applied DOB in pneumatic systems and achieved improved control under varying load conditions. Ramezani-al et al., (2023) further combined DOB with sliding mode control, achieving enhanced system stability.

Nigus, (2018) reported that, in piston-type air compressors, fluctuations in crankshaft speed under varying loads or excitations cause changes in inertia forces among the moving components, unlike in constant-speed operations. Zhao et al., (2023) observed that many welded plate structures in the compressor installation base exhibit weak stiffness, low damping,

and a tendency toward vibration radiation when subjected to excitation. Kang et al., (2018) highlighted that vibrations generated by air compressors contribute to mechanical wear, performance reduction, and safety risks. Žiaran et al., (2020) asserted that reducing the dynamic load of machinery with respect to its surrounding environment and operators enhances safety, reliability, and longevity, while also reducing emissions, mechanical vibrations, and noise, thereby improving the working environment.

Khan & Burdzik, (2023) noted that vibration frequencies within the range of 10 to 250 Hz could disrupt sleep, increase stress levels, and potentially cause irregular heartbeats in operators. Kostyukov & Naumenko, (2016) experimentally determined that piston-cylinder assemblies account for more than 30% of all malfunctions, with ring failures alone comprising over 25%. Furthermore, Ghazwani and Pham, (2024) reported that significant failure rates occur in both slide-crank and cranking mechanisms. Carletti and Pedrielli, (2019) emphasized that noise and vibration levels pose a considerable health risk to operators and vary significantly in magnitude.

It was noted that piston-type compressors were generally not equipped with vibration suppression control systems. Faris et al., (2019) concluded that developing a robust control system for vibration suppression has the potential to considerably extend the operational lifespan and reliability of such compressors. On this basis, the dissertation focused on modelling and developing a robust control system designed to meet the specific operational demands of piston-type air compressors.

### 1.2 Problem Statement

Piston-type air compressors inherently exhibit significant vibration levels, particularly during pump operation, due to the periodic and nonlinear forces introduced by the exhaust and suction cycles. These cyclic disturbances act as primary sources of system instability, adversely affecting the dynamic behavior of the compressor assembly. Recent investigations (Zhang et

al., 2021) have shown that pressure and airflow fluctuations induced by these vibrations lead to persistent energy inefficiencies and operational irregularities, resulting in considerable economic losses across various industrial applications. Furthermore, elevated vibration levels accelerate structural degradation, causing premature wear of mechanical components and reducing overall system reliability. Notably, Wang et al. (2022) identified gas pulsation and structural resonance as dominant contributors to pipeline fatigue, leakage, and heightened safety risks within compressor systems. In addition to mechanical deterioration, the resulting acoustic noise negatively impacts workplace conditions, reducing productivity and posing long-term health risks to personnel. Although some advancements in air compressor design were made, current technologies have not adequately addressed the underlying dynamic instabilities. This underscores the necessity for the development of robust control strategies aimed at effectively suppressing vibration, thereby enhancing system stability, reliability, and operational efficiency.

## 1.3 Research Objectives

### 1.3.1 Main Objective

The main objective of the study was to model and develop a robust control system for vibration suppression of piston-type air compressors.

### 1.3.2 Specific Objectives

The specific objectives of the research are:

i) To derive an accurate dynamic model of a piston-type air compressor that captures the key sources of vibration.

ii) To develop and apply a Disturbance Observer-Based (DOB) control strategy for real-time suppression of vibration in piston-type air compressors.

iii) To validate the performance of the proposed control system through simulation analysis.

## 1.4 Scope of the Project

The scope of the research included mathematical modeling, a comprehensive analysis, and simulation-based approach that addressed vibration challenges encountered by air compressors in industrial environments. This included a detailed examination of the existing compressor system, development of mathematical models, design of advanced control system, and validation of their performance using MATLAB/Simulink software. While focusing on simulation-based analysis and validation due to time and financial constraints, the research aimed at optimizing compressor operation through the integration of motor position control mechanisms.

## 1.5 Significance of the Research

The research was considered to hold significant importance in the context of industrial productivity, energy efficiency, technological innovation, and environmental sustainability. It was reported that by focusing on the design and implementation of advanced control systems for air compressors, the research aimed to address critical challenges faced during industrial operations, such as downtime, energy wastage, and environmental impact. The study indicated that by optimizing air compressor performance through advanced control strategies, the research aligned with Uganda's Vision 2040, which emphasizes the role of industrial development in driving economic growth and transformation (Namata, 2023).

Furthermore, it was noted that by leveraging cutting-edge technologies, the research contributed to technological innovation and capacity building in Uganda's manufacturing sector, fostering a culture of innovation and knowledge-driven growth. Ultimately, the findings were suggested to have the potential to enhance industrial productivity, reduce energy consumption, and support Uganda's vision for sustainable economic development and global competitiveness.

# CHAPTER TWO: LITERATURE REVIEW

## 2.1 Introduction

This chapter examined the relevant literature on the design, control, and optimization of air compressor systems, with a particular emphasis on motor dynamics control and pressure regulation. By reviewing existing research and approaches, this study sought to identify knowledge gaps and lay the basis for the suggested control system design.

### 2.1.1 Case Example of the Compressor System

Figure 2.1 presented a piston type air compressor system utilized to supply compressed air at Geotechnical Engineering and Technology Laboratory Limited (GETLAB LTD).

### 2.1.2 General Layout, Composition, and Functionality

The air compressor system shown in Figure 2.1 was a piston-type (reciprocating) model, featuring a fully enclosed design with fan cooling. It was a multipart assembly of interconnected components, each playing a crucial role in the compression and delivery of pressurized air. During its operation, it drew in air under atmospheric conditions and compressed it to the desired pressure level. This process took place by mechanical action and thus, converting the motorized energy transmitted via the belt into hydraulic energy. The power applied to the air increased its energy per unit volume.

Pipalia et al., (2016) investigated that, the transfer of heat to and from the gas was determined from two mechanisms “suction air heating” and “discharge air cooling.” In addition, prior to entering the cylinder, radiation heated the suction pipes, followed by conductive and convective heating as the air traveled through the cylinder and valve passages. Consequently, the air temperature inside the cylinder rose as the pressure increased during the suction stroke. The air was heated and returned during suction and throughout most of the expansion stroke. Although heat exchange between the gas and the cylinder occurred continually, there was no net transfer

of heat between the compressor system and its surroundings. Therefore, a power link was established between the air molecules within the pump and the change in mechanical energy.

The compressed air was stored in a tank, providing an on-demand power source for pneumatic tools and equipment, as shown in Figure 2.1 In this setup, the compressor maintained a minimum air pressure of 800 KPa in the storage tank, restarting if the pressure fell below this pressure. Additionally, the compressor maintained a minimum storage tank pressure of 800 kPa, restarting if the pressure dropped below this threshold, and limiting the output pressure in the hose pipes to a maximum of 800 kPa. During its operation, the piston type air compressor converted power from the electric motor into potential energy. With the help of the suction valves, atmospheric air at 14.5038 psi was drawn in and stored inside the compressor's storage tank, where it was compressed by the pistons from 100 psi to 150 psi.

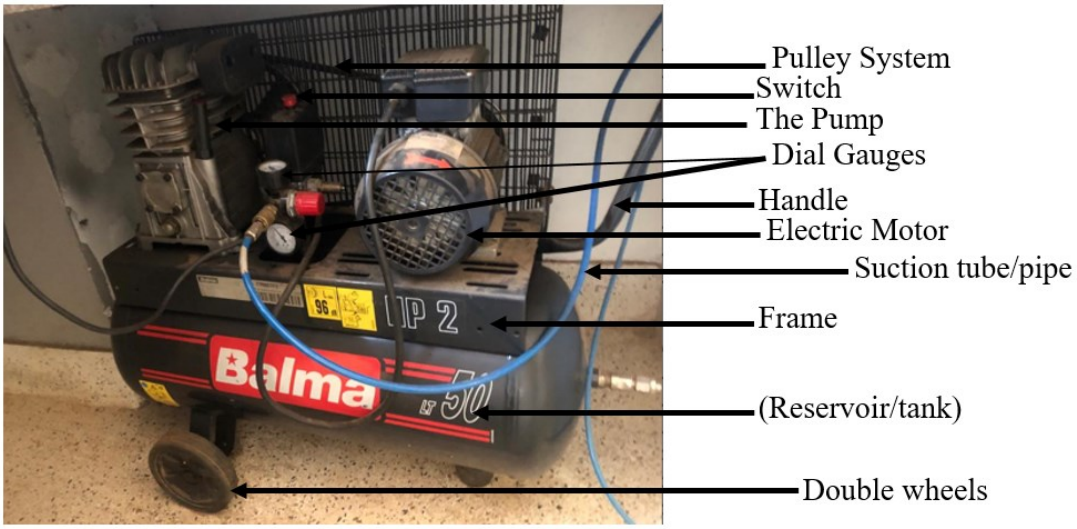


**Figure 2.1: Typical piston-type air compressor**

From the compressor tank, the compressed air was distributed via a network of pipes or hoses to the two-automatic consolidation oedometer and shearmatic machines, as shown in Figure 2.2. The pressure regulation system consisted of two gauges: one set to a maximum pressure of 150 psi for the compressor tank, and the other connected to the equipment to maintain a desired pressure of 116.03 psi for successful test operation. It was noted that before reaching the

equipment, the compressed air was filtered to remove contaminants via condensation and cooled to acceptable testing temperatures.

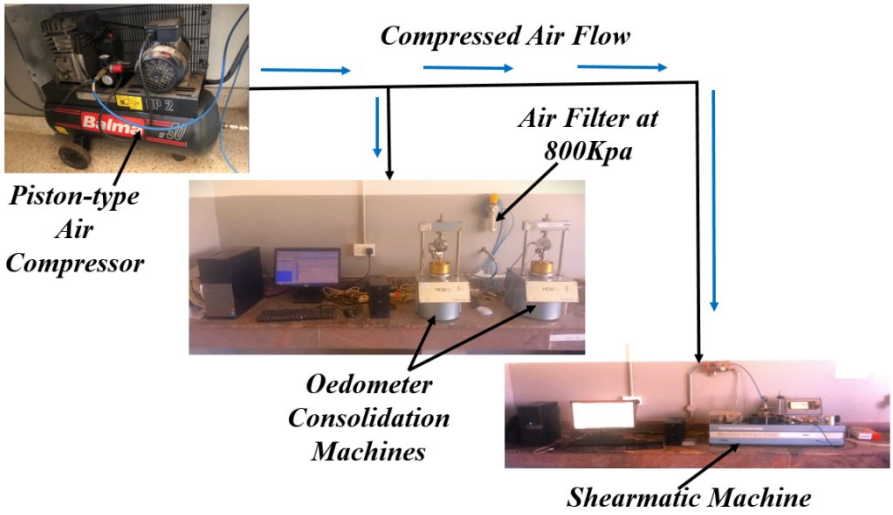


**Figure 2. 2: Layout of compressed air flow from the piston-type air compressor to the equipment**

### 2.1.3 Air Compressor Operating Conditions and Vibration Challenges

According to Mi & Meng, (2014), the compressor motor drives the crankshaft to rotate through the coupling. It was reported that the crankshaft, fitted with two connecting rods, drove the reciprocating motion of two pistons inside the compressor tank (Cheng & Liu, 2017). Additionally, Marvania & Subudhi, (2017) explained that the gas was compressed in stages as the rotational mechanical energy was converted into the pressure energy of air. It was stated that reciprocating, or piston-type, air compressors were widely preferred for applications requiring very high pressures and for handling light gases such as hydrogen or hydrogen-rich mixtures (Almasi, 2016). An investigation by Jani et al., (2019) highlighted that a double-acting reciprocating air compressor could achieve a volumetric efficiency of 86%, maintaining consistent compressed air flow rates across a wide output range. More still, condition monitoring relied on parameters such as vibration, flow, power, position, temperature, and

pressure, with the choice of measurements based on the observed faults to ensure effective diagnostics (Townsend et al., 2016).

Zhang et al., (2017) observed that the compressor body was subjected to irregular alternating loads due to the periodic action of the exhaust and suction valves, which Liang et al., (2015) identified as a major cause of compressor vibration. Further research by Chu et al., (2024). indicated that excessive vibration reduced efficiency by causing wear on structural components, eventually leading to damage to the system unit.

System vibrations were observed when the tank pressure fell below 800 kPa, prompting the compressor to draw in more air to compress it to the required 1268 kPa for operating the three machines, as shown in Figure 2.2. The belt system transferred power from the electric motor to the air pump, which driven by electricity, supported the compression process by filling the tank with air (Amiebenomo et al., 2023).

The engine's power output was transmitted to the air pump via a belt drive system by ensuring efficient power transfer and synchronization of operation (Sriraman, 2023). The electric motor assisted in starting the air compressor and sustaining stable operation during use (Caruana & Refalo, 2018). The compressor's frame provided a stable foundation for the entire assembly, while the hoses and fittings were built to withstand pressure fluctuations and facilitate the distribution of compressed air from the tank to various outlets and applications (Amiebenomo et al., 2023).

Despite this functional design, the piston-type air compressors faced significant challenges due to operational conditions and inherent design limitations. Operating at high-pressure was associated with high-amplitude vibrations and that interconnected parts, such as the compressor's valve plate, were prone to premature damage, loosening, and breakage. For instance, Yin et al., (2020) reported that the most common failing elements in compressor

cylinder systems were the suction and discharge valves with percentage of 29.1% and 21.6%, respectively. In addition, it was stated that electromagnetic vibration, mainly expressed as high-frequency amplitude from the motor, was caused by electromagnetic forces producing torque, which in turn deformed the stator and vibrated the rotor. The study explained that this noise and vibration depended on the motor's electromagnetic parameters and control mode. Such vibrations contributed to equipment fatigue, premature failure, disruption of nearby workstations, and operational challenges. Hu et al., (2022), further emphasized that vibration accelerated fatigue damage, increased energy consumption, caused discomfort, and could even harm human health.

Vibrations could propagate through the compressor's structure, affecting the stability and precision of key components such as the electric motor and belt drive system. Hong et al., (2023) found that noise and vibrations in electric motors were often linked to the coupling condition with the load and poor installation, with factors such as misalignment, external stresses from connected equipment, and faulty foundations contributing to the problem. The absence of precise control mechanisms represented a fundamental limitation in the compressor's performance. Without adequate control over motor position or speed, the compressor operated inefficiently, leading to energy wastage, inconsistent output, and increased operational costs. This deficiency also hindered the compressor's ability to respond dynamically to changes in demand, resulting in suboptimal performance and reduced overall productivity.

In summary, the air compressor in Figure 2.1. operated under challenging conditions characterized by noise, vibration, and inadequate control mechanisms. These factors caused significant challenges to its performance, reliability, and efficiency, highlighting the need for targeted interventions and innovative solutions to enhance its functionality and optimize its operation.

### 2.1.4 Overview of Air Compressor Systems

Nourin et al., (2022), stated that compressed air is vital for many industrial processes and that boosting compressor air efficiency is a top goal in today's industry to improve product quality, enhance productivity, and save energy. Smith (2018) highlighted that air compressors were classified into reciprocating, rotary screw, and centrifugal types, each offering distinct advantages in terms of efficiency, reliability, and cost-effectiveness. Air compressor systems were essential to many mechanical and industrial applications because they lowered the volume of a gas while increasing its pressure (Ben Mansour et al., 2014). Air compressors converted energy from an electric motor or engine into stored compressed air or gas, which powered pneumatic tools, cooling systems, and industrial processes (Marvania & Subudhi, 2017).

### 2.1.5 Key Components of an Air Compressor System

A report by Amiebenomo et al., (2023) showed that compressor systems consist of multiple components, including the air pump, engine, belt or screw drive system, motor, tank, control mechanisms, and associated piping. These systems varied in complexity and design, depending on the intended application and operational requirements. The air intake filter plays a crucial role in maintaining the efficiency and longevity of an air compressor. Maduna & Patnaik, (2017) reported that filtering out contaminants such as dust and debris prevents these particles from entering the compression chamber, which could otherwise cause wear and tear, reduce the compressor's performance, and potentially lead to mechanical failures.

The compression chamber serves as the core component of the compressor system, where the actual process of air compression occurs. In this chamber, air is confined and compressed either by a piston in reciprocating air compressors or by a rotor in rotary air compressors (Marvania & Subudhi, 2017). The reduction in volume increases the pressure of the air. The compressor is powered by a motor or engine, which transforms electrical or chemical energy into mechanical energy necessary for the compression process. Stationary air compressors typically

utilize electric motors, whereas portable air compressors are generally equipped with diesel or gasoline engines (Li et al., 2015).

The compressed air is stored in a storage tank, also known as a receiver, which ensures a steady supply (Ben Mansour et al., 2014). The pressure regulator manages the output pressure of compressed air, guaranteeing that it is supplied at the necessary pressure level for the particular application. This device plays a crucial role in ensuring stable performance and safeguarding downstream equipment (Wasbari et al., 2017). The control system monitors and manages the operation of the compressor (Gupta et al., 2020). It includes pressure sensors, temperature sensors, and control valves that ensure the compressor operates within its design limits, maintaining efficiency and safety.

Air compressors produce considerable heat while functioning. A cooling system is used to dissipate heat, preventing overheating and ensuring the compressor operates efficiently (Marvania & Subudhi, 2017). The lubrication system guarantees the smooth operation of moving components within the compressor, including pistons and rotors (Maduna & Patnaik, 2017). Adequate lubrication reduces friction, decreases heat production, and reduces wear, thereby prolonging the lifespan of the compressor. Vibration dampers minimize the vibrations caused by the moving parts of the compressor. Excessive vibration lead to mechanical failure or noise issues, so damping systems are crucial for stable operation (Zhao et al., 2019). The discharge line carries the compressed air from the storage tank to the point of use. This line often includes a check valve to prevent backflow, ensuring that air flows only in one direction (MWE, 2013).

### 2.1.6 Classification of Air Compressors

Air Compressors are broadly classified into positive displacement and dynamic compressor types (Amiebenomo et al., 2023) as indicated in Figure 2.3. Positive displacement air

compressors operate by compressing gas to decrease its volume, thereby elevating its pressure. These compressors are generally classified into two primary types: rotary and reciprocating air compressors (Lu et al., 2023). Reciprocating air compressors function by employing a piston that compresses air inside a cylinder; each movement of the piston lowers the volume while simultaneously elevating the pressure (Nourin et al., 2022).

Reciprocating air compressors are divided into two categories: single-acting and double-acting. As noted by Pipalia et al., (2016), double-acting air compressors enhance efficiency by compressing more air per cycle, while single-acting compressors compress air during only one stroke of the piston. Additionally, single-stage reciprocating air compressors are suitable for low-pressure applications, whereas multi-stage air compressors are preferred for high-pressure needs. Reciprocating air compressors are widely utilized in refrigeration and air conditioning systems, natural gas processing, oil refineries, and plastic bottle manufacturing.

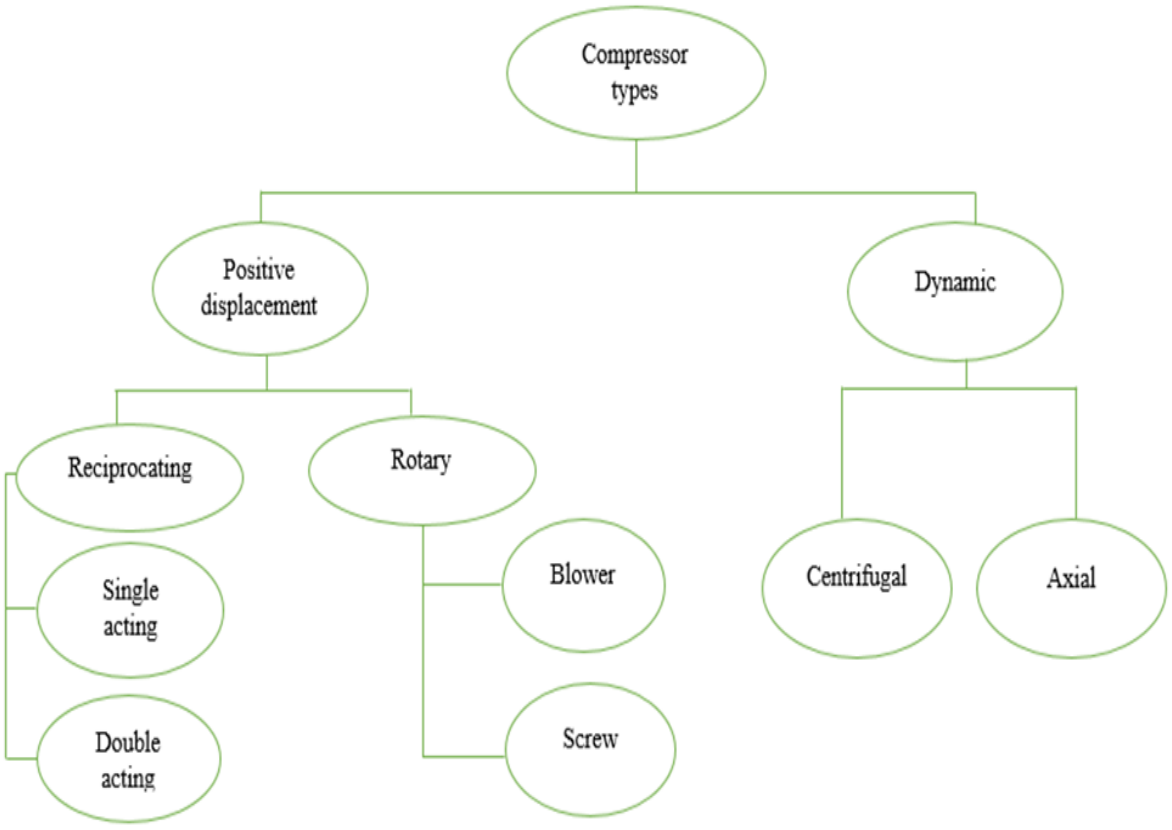


**Figure 2.3: Classification of air compressors, source (Junedi, 2020)**

A reciprocating stroke compressor is a specific kind of air compressor that operates by compressing air within a cylinder. This process involves moving the air upward to the top dead center (TDC) and drawing in external air as the piston descends to the bottom dead center (BDC) of the cylinder, (L) represents the length of air travelled through the section between (TDC) and (BDC) as depicted in Figure 2.4.

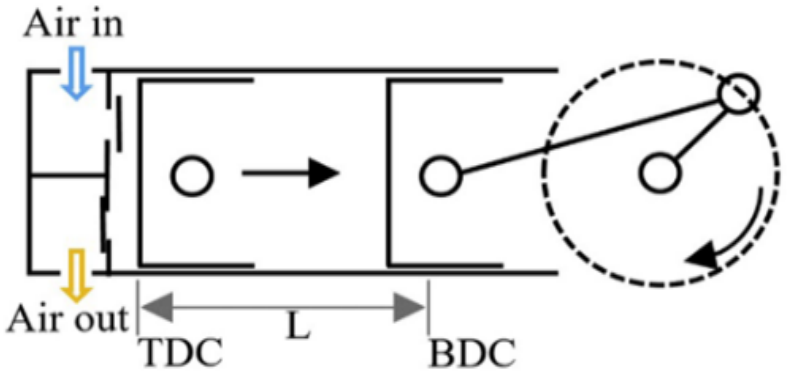


**Figure 2.4: Fundamental concept of a piston-type or reciprocating air compressor (Tempiam et al., 2020)**

Rotary air compressors operate by utilizing rotating components, such as rotors, to achieve air compression. These air compressors are primarily categorized into two main types: rotary screw and rotary vane air compressors (Ben Mansour et al., 2014). Rotary screw air compressors operate by employing two helical rotors that rotate in opposing directions, facilitating the compression of air as it passes through the compressor (Marvania & Subudhi, 2017). Rotary vane air compressors function by using rotating vanes that move in and out of slots on a rotor to compress air (Aw & Ooi, 2021). In their study, Aw & Ooi, (2021) also found that the rolling piston compressor, a type of rotary machine, has better vibrational performance than the reciprocating compressor. They further explain that although the rolling piston compressor offers improved vibrational characteristics, the presence of an eccentric cam and its orbiting motion can still cause vibrations. These can be reduced by using dampers and/or rotational balancing methods.

Dynamic air compressors operate based on an alternative principle, utilizing a continuous airflow to create pressure instead of compressing the gas volume. They are generally categorized into centrifugal and axial air compressors (Amiebenomo et al., 2023). Centrifugal air compressors operate by utilizing a rotating impeller to enhance the air's speed, subsequently transforming it into pressure via a diffuser (Nourin et al., 2022). These air compressors are extensively utilized in substantial industrial settings owing to their exceptional efficiency and capacity to manage significant air volumes (Lu et al., 2023). In a steady-flow process, air enters the centrifugal compressor, where the vapor traverses the impeller blades and experiences centrifugal force. Ultimately, the fluid exits the compressor via the diffuser at the designated outlet pressure.

### 2.1.7 Advantages and Disadvantages of Centrifugal Air Compressors

Centrifugal air compressors offer several advantages, including minimal noise operation, high efficiency levels ranging from 72% to 85%, and a longer lifespan due to having fewer moving parts compared to reciprocating air compressors (Tiainen et al., 2018). They are capable of operating across a wide range of rotational speeds, typically starting at 3000 rpm, and provide higher flow rates than positive displacement air compressors (Meroni et al., 2018). However, they also have some drawbacks. One significant issue is surging, which occurs when a decrease in refrigeration load causes refrigerant to flow back from the compressor to the evaporator (Wang & Yan, 2024). Additionally, achieving a high compression ratio is more challenging for centrifugal air compressors, as the pressure increase per stage is lower compared to reciprocating air compressors (Shu et al., 2019).

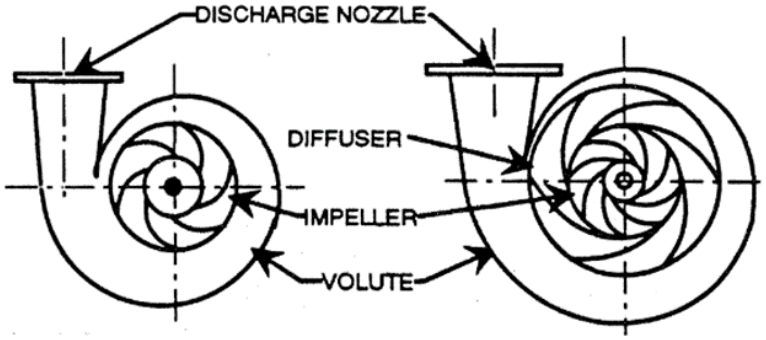


**Figure 2. 5: Operational mechanism of centrifugal air compressors (Robison & Beaty, 2013)**

Axial air compressors operate by compressing air that moves axially through a sequence of rotating and stationary blades. These air compressors are typically employed in scenarios demanding exceptionally high flow rates, such as in jet engines or large-scale power generation facilities (Ben Mansour et al., 2014). As noted by Aboelhassan et al., (2020), axial air compressors are uncommonly utilized in smaller commercial applications because of their intricate design and elevated expenses. In addition, the prediction of axial flow compressor performance is linked to various complexities and challenges as observed by Peyvan & Benisi, (2016).

Axial air compressors are classified as dynamic machines that facilitate the acceleration of gas flow in both axial and peripheral directions through the rotation of uniquely designed blades. The flow of the process is aligned with the centerline of the shaft. The stator blades play a crucial role in converting speed into pressure. According to Amiebenomo et al., (2023), an axial flow air compressor exhibits superior efficiency compared to a centrifugal type.

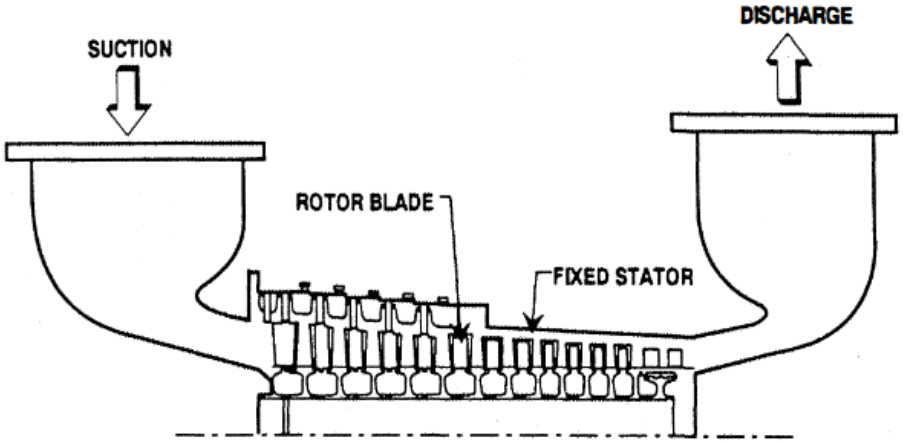


**Figure 2.6: Axial air compressor (Robison & Beaty, 2013)**

## 2.2 Major Causes of Vibration in Air Compressors

All machines vibrate during operation, regardless of how securely they are installed. This vibration is caused by different forces and can lead to undesirable motion in the machine and its attached components. Air compressor vibrations often transfer through belts and structural components as stated by Eklind, V., & Karlsson, (2019). Additionally, any defects in rotating transmission elements, like eccentricity, can cause vibrations at the main rotational frequency and possibly at higher harmonics. If this movement becomes excessive, it can cause damage to the machine. Tran et al., (2014) investigated that air compressors, particularly the reciprocating type, consist of numerous components that move in both rotary and linear motions, resulting in a vibration signal that is non-stationary and characterized by noise.

Furthermore, the overall vibration noise level of an air compressor arises from unbalanced inertia and torque in the crank-connecting rod assembly, overturning torques from gas forces, motor-induced vibrations, and the cyclic intake and exhaust processes (Chai et al., 2023). The moment of inertia of a crank mechanism, which varies throughout the crankshaft's rotation, plays a crucial role in implementing the proposed dynamic control method effectively (Egorov et al., 2019). Bearings are installed on the housing to give the shaft axial and radial support (Krot et al., 2020).

The first sign of many problems in the air compressor system will be vibration in the crankshaft or bearing housing (Zhang et al., 2014). The imbalance in the engine can lead to the generation of unbalanced dynamic mass forces due to the reciprocating and rotational masses (Hoag & Dondlinger, 2015). For instance, pulsation forces (caused by the forth and back flow of the piston as well as during suction and discharge strokes, flow starts and stops suddenly, causing pressure fluctuations), gas forces within the cylinder, torsional forces, lateral forces, and forces exerted by the cross-head guide (Kacani, 2017). Vibration resulting from fluid dynamics is caused by the behavior of fluids, including occurrences such as turbulence, variations in pressure, or pulsations (Ben Mansour et al., 2014).

The modeling of pulsation and pressure variations is accomplished through the application of the continuity and momentum equations related to compressible fluid dynamics (Marvania & Subudhi, 2017). Resonance takes place when the natural frequency of the compressor coincides with the frequency of the vibration source, resulting in amplified vibrations (Maduna & Patnaik, 2017).

### 2.3 Sources of Friction in Air Compressors

A study conducted by Mantri & Tamma, (2014) clarifies that the friction occurring in reciprocating air compressors arises from the interaction between the piston and the cylinder, the friction related to the valves, and the bearings that provide support to the crankshaft.

### 2.4 Motor Components

Utilizing equipment in proximity to resonance frequencies, particularly with the implementation of adjustable speed drives, may lead to significant vibrations (Mohd-Ghazali & Rahiman, 2021). The researchers further noted that inconsistencies in the magnetic field contribute to vibrations. Additionally, Lipus et al., (2016) stated that the friction between the

rotor and stator, or other rotating components within the motor, can lead to vibrations, particularly in cases of misalignment or imbalance.

### 2.4.1 Air Compressor Components

In reciprocating air compressors, the friction occurring between the pistons and cylinders significantly contributes to vibrations. Irregular wear patterns or inadequate lubrication can increase friction levels, causing inconsistent movements that ultimately result in vibrations (Söderfjäll, 2017).

Friction within air compressor elements such as belts or gears may lead to vibrations in addition to misalignment or inadequate tension which can further intensify this problem (Eklind, V., & Karlsson, 2019). In addition, Porwal, (2015) highlights the impact of valve friction in generating vibrations within air compressors, noting that friction arising from the operation of inlet and discharge valves can lead to vibrations as a result of wear, accumulation of debris, or inadequate maintenance practices. A study conducted by Muzakkir & Kumar, (2015) proves that the presence of friction at seals and gaskets leads to vibrations, especially when they are not operating effectively due to wear or incorrect installation.

## 2.5 Modelling and Simulation of Air Compressor Systems

System dynamics (SD) is a comprehensive methodology based on feedback control theory, designed to tackle nonlinear systems and facilitate computer simulation ( Yin et al., 2024). The techniques for modeling and simulation are essential for comprehending the dynamic behavior and performance attributes of air compressor systems (Zhang et al., 2018).

Olabi et al., (2021) showed how dynamic simulation models are used in utilizing principles of thermodynamics and fluid dynamics to analyze compressed air systems across different operating conditions. Works by Kotlov, (2019) provide extensive insights into developing mathematical models of a two-stage reciprocating compressor by methods of physical and

mathematical experiments whereas Kavya & Jayalalitha, (2022) demonstrate how computational simulations can be utilized to optimize control strategies to improve maximum power point tracking in a photovoltaic system.

MATLAB/Simulink–based simulations are frequently employed to model motor dynamics, control algorithms, and system interactions, offering significant insights into the behavior of systems across various operating conditions (Halicioglu et al., 2014).

### 2.6 Motor Position Control in Air Compressor Systems

Motor position control is essential for maintaining precise operation and efficiency in air compressor systems. Literature in this area includes a wide range of approaches, including sensor-based feedback control, model-based predictive control, and disturbance estimation techniques. According to Zhang and Li (2019), disturbances such as vibrations and mechanical coupling significantly affect motor position control performance, emphasizing the need for robust control algorithms and advanced sensing technologies.

### 2.7 Vibration Control Strategies for Air Compressor Systems

Vibration suppression is crucial for safeguarding precision instruments against excessive vibrations. Linear vibration isolators operate effectively at excitation frequencies that exceed $\sqrt{2}$ times the peak frequency (Lu et al., 2020). The comprehensive design of the integrated nonlinear passive vibration control system must take into account the loading capacity as well as the performance of vibration isolation and absorption, as examined by Jiang et al., (2021).

Further studies suggest that the incorporation of nonlinearity into certain conventional vibration isolation structures can significantly enhance their vibration isolation capabilities in engineering applications (Lu et al., 2020). The optimal isolation performance is typically attained through the integration of a tilt horizontal coupling immune inertial double link sensor for low frequency applications (Nair et al., 2024).

A subsequent review conducted by Chen et al., (2016) introduced two innovative control techniques derived from the disturbance observer framework, namely the “fast disturbance observer” and the “slow disturbance observer,” aimed at achieving “resonance ratio control.” It was noted that the fast disturbance observer demonstrated superior performance across a broad spectrum of inertia ratios. A straightforward two-degree-of-freedom (DOF) PID controller is employed for Pole Zero Control (PZC) to manipulate the zeros of a reference transfer function. The PZC technique is implemented in both a spring-mass system and a two-mass resonant system to mitigate vibrations, demonstrating effectiveness in each scenario (Urakawa, 2019). Samuel et al.,(2024) discuss a Multi-function Observer (MOB)-based control scheme designed to enhance motion control accuracy by directly suppressing disturbances. This approach also improves outer-loop admittance control shaping in industrial robots.

Strategies for controlling air compressors play a crucial role in improving system performance and efficiency. According to Aboelhassan et al., (2020), the techniques for vibration suppression are classified into two main types: passive methods and active methods. Techniques for active control, including PID controllers, model predictive control (MPC), and adaptive control methods, are widely utilized for the purpose of vibration suppression (Salem et al., 2015). In their study, Gupta et al. (2020) studied the application of MPC for controlling air compressor systems by demonstrating improved energy efficiency and system stability compared to the conventional control methods. Furthermore, MPC enhances energy efficiency and stabilizes the system in air compressor applications (Gupta et al., 2020). Similarly, adaptive controls are essential in industrial processes as they adjust parameters in real-time, ensuring safety, efficiency and stability (Aboelhassan et al., 2020). Model Predictive Control (MPC) is a multi-input/multi-output strategy that adjusts various inputs to control multiple outputs. By inverting the process model, MPC manages each output by dynamically adjusting the inputs to meet desired outcomes ( Samuel & Parthiban, 2016).

Martinez-García, et al. (2020) show that the majority of commercial motion controllers available for industrial processes are built on the foundation of PID (proportional-integral-derivative) controllers and other classic controllers. These controllers are systems with a closed architecture. AbdulKareem,(2018) demonstrates that a fuzzy adaptive PID control based on the cascade control system is used to analyze the characteristics of steam pressure-controlled objects. Veysi et al., (2024) also describe the PID controller as a combination of Proportional, Integral, and Derivative actions to provide a balanced approach to correcting error, eliminating steady-state error, and predicting future errors.

### 2.8 Research Gaps

The vibration issue stems from the fundamental mechanical dynamics of air compressors especially those of the reciprocating variety which arises due to the fluctuating loads linked to the suction and exhaust phases. If these vibrations are not effectively managed, they can result in reduced operational efficiency, structural degradation, and intensified maintenance expenses. Furthermore, excessive vibrations pose a risk of damaging critical components, including the motor, crankshaft, and connecting rods, thereby jeopardizing the overall performance of the compressor.

Based on the above gaps, there is limited literature on control system design for piston-type air compressors, especially concerning the use of control mechanisms to suppress disturbances and vibrations.

This research focuses on developing a robust control system for the piston-type air compressor system. This is unique because the system involves incorporating a control mechanism as a tool used to stabilize the entire compressor unit. This system incorporates a blend of actuators and control algorithms aimed at dynamically modifying the operating parameters of both the compressor and the motor to ensure stability. By addressing variables such as motor torque,

rotational speed, and air pressure in real-time, the control system effectively minimizes the mechanical stress induced by vibrations.

**Table 2.1:Summary of Related Studies, Gaps, and Contributions of the Study**

| **Study / Source** | **Identified Limitation** | **How the Study Addresses the Gap** |
|---|---|---|
| Sun et al. (2025) | Mechanical modelling without integration of control for vibration suppression | Integrates a unified mechanical-control model with DOB-based control for active vibration mitigation |
| Bezrukovs et al. (2024) | Nonlinear valve and seal dynamics are modeled via CFD but excluded in linear frameworks | Acknowledges nonlinearity and proposes control design robust to such dynamics |
| Zhang et al. (2025) | Inerter-based suppression lacks robust control integration | Implements DOB, a robust control strategy under varying load conditions |
| Chernyi et al. (2021) | Torsional vibration in crank-drive systems is not considered in typical models | Includes equivalent inertia modelling capturing torsional effects in system behaviour |
| MDPI (2022) | Material damping via super-damping rubber lacks integration into active control systems | Suggests future experimental integration of passive and DOB-based active control |
| General Literature Review | Adaptive and DOB control methods rarely applied to piston compressors | Introduces DOB control specifically adapted for dynamic compressor environments |
| MDPI Review on Linear Compressors (2022) | Highlights lack of hardware-in-the-loop (HIL) or prototype validation | Recommends HIL and real-time testing as a future direction to validate model |
| MPC in Cryocoolers (2023) | MPC rarely used in piston compressors despite MIMO nature | Proposes using DOB control as a practical foundation for future MIMO/MPC applications in piston systems. |

# CHAPTER THREE: METHODOLOGY

## 3.0 The Conceptual Framework of the Study

The conceptual framework of this research was presented in Figure 3.1. It illustrated the compressor system and controller operating within a feedback loop. The methodology for each component of the study was structured based on the specific research objectives.

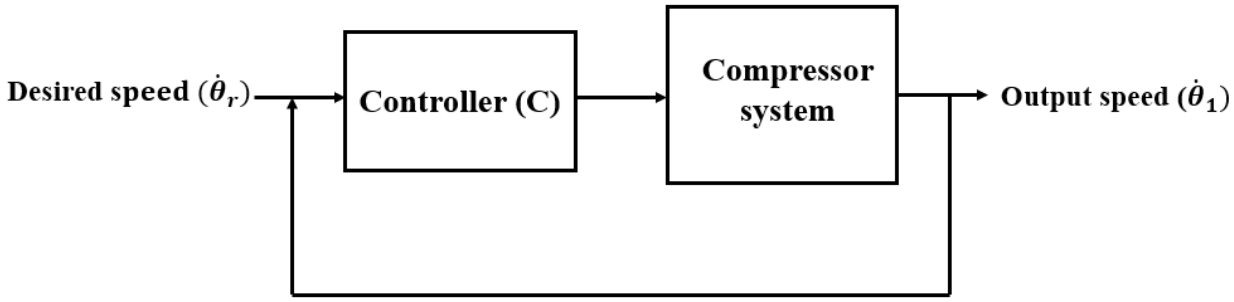


**Figure 3.1: Conceptual framework of the study**

## 3.1 System Modelling

### 3.1.1 Mathematical Modelling of the Compressor System

The compressor system consisted of an electric motor used to power the piston compressor. A mathematical model of the motor was developed, incorporating its speed characteristics and dynamic properties such as inertia, friction, and electrical behaviour. Additionally, the compressor side was modelled, and a general transfer function was derived by combining the dynamics of the entire system.

### 3.1.2 Determination of the Parameters

Based on the mathematical model, the key system parameters -including the inertia and damping coefficients of both the electric motor and the compressor load -were determined accordingly.

### 3.2 Control System Design Procedure

The established mathematical model was used to design a control system for regulating the dynamic performance of the piston compressor system, while an initial uncontrolled model was formulated to evaluate the system's response to disturbances. Subsequently, a control system incorporating disturbance estimation was implemented to evaluate system performance and mitigate the impact of disturbances. This involved the integration of a disturbance observer (DOB) to handle external disturbances, such as mechanical vibrations, in a feedforward manner.

The control design utilized active control techniques, including PID control and state feedback control, to improve system tracking performance. The design was structured into two main components: the reference tracking component and the disturbance rejection component. Additionally, nominal system parameters and the system's cut-off frequency were considered in the design. Reference tracking was achieved by comparing the desired speed reference (set-point) with the measured output speed. Control computations were performed using a PID algorithm to generate the control signal that minimized the error between the desired and actual speeds.

#### 3.2.1 Design Procedure for a Piston-Type Air Compressor Control System

The steps taken in designing the control system were represented as indicated in Figure 3.2.

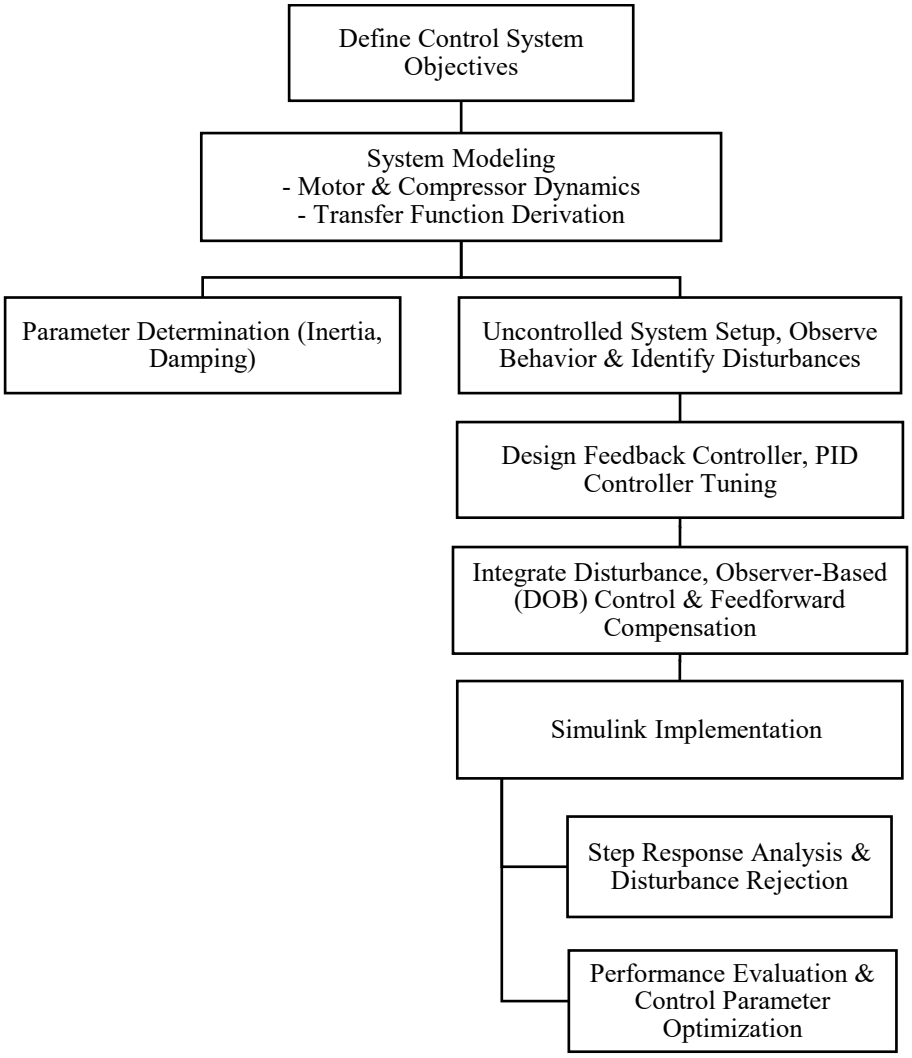


**Figure 3. 2: Flow-chart - control system design**

### a. Definition of the Control System Objectives

The primary objective of the control system was to ensure precise tracking of the compressor motor's desired speed or position while actively minimizing vibrations caused by dynamic disturbances. This was achieved through a well-designed control strategy that enhanced system stability, delivered a fast response to input changes, and reduced overshoot, thereby ensuring reliable and efficient compressor performance.

### b. System Modelling and Control Design

The control system development commenced with mathematical modelling of the motor-compressor system, capturing key dynamics such as torque generation, mechanical inertia, and

damping effects. Transfer functions were derived to represent input-output relationships, forming the foundation for simulation and control design.

**c. Parameter Determination**

Critical system parameters including rotor and crankshaft inertia, as well as damping coefficients were estimated or experimentally determined to ensure accurate modelling and effective control tuning.

**d. Uncontrolled System Setup, Observe Behavior and Identify Disturbances**

An initial uncontrolled model was simulated to observe the system's inherent behaviour and identify internal and external disturbances arising from reciprocating motion and unbalanced forces.

**e. Designing and Tuning of Feedback controller**

Based on these insights, a Proportional-Integral-Derivative (PID) feedback controller was designed, with gains tuned to enhance responsiveness, minimize overshoot, and maintain stability.

**f. Integrate Disturbance, Observer-Based (DOB) Control and Feedforward Compensation**

System robustness was further improved by integrating a Disturbance Observer-Based (DOB) strategy alongside feedforward compensation, enabling real-time disturbance rejection and proactive mitigation of predictable perturbations.

**g. Simulink - based Implementation**

The complete control architecture, including models and algorithms, was implemented in MATLAB/Simulink, facilitating block-diagram simulation under various operating conditions. Dynamic performance was evaluated using standard input signals, assessing key metrics such

as rise time, settling time, overshoot, and steady-state error, while also verifying disturbance rejection capabilities.

**h. Performance Evaluation and Control Parameter Optimization**

Finally, iterative simulation and tuning refined the control parameters to optimize vibration suppression, response time, and robustness across varying load conditions, achieving a balanced and stable system performance.

### 3.3 Model Implementation and Controller Validation using MATLAB/Simulink:

#### 3.3.1 Model Implementation

A complete simulation model of the compressor system was developed in MATLAB/Simulink, and the model's accuracy was verified by comparing the simulation results of the actual system with those of the estimated or equivalent model. Moreover, control algorithms-including motor torque control, disturbance rejection, and cut-off frequency tuning-were implemented within the Simulink environment, and the controller parameters were systematically tuned in order to enhance system performance and stability.

#### 3.3.2 Controller Validation

Validating the designed control system using real-time simulations in MATLAB/Simulink was achieved.

#### 3.3.3 Simulation Studies

These were conducted to evaluate the performance of the designed disturbance observer-based control system under various operating conditions. The key performance metrics analysis such as tracking accuracy, stability, and disturbance rejection was done.

### 3.4 Performance Evaluation and Optimization

#### 3.4.1 Performance Metrics

The control system was evaluated using predefined performance metrics, including tracking accuracy, system stability, cut-off frequency, and effectiveness in disturbance rejection.

### 3.4.2 Optimization

System optimization involved fine-tuning the control parameters based on simulation results to further enhance overall system performance and efficiency.

# CHAPTER FOUR: RESULTS AND DISCUSSION

## 4.1 Modelling of the Compressor System

### 4.1.1 Overview of the Compressor System

It was important to understand the interaction between the motor and the load/compressor in order to improve on the performance and efficiency of the compressor system. Additionally, it was important to develop compressor mathematical models that addressed system vibrations. In this context, the load/compressor was associated with several mechanical components, including the crankshaft, connecting rods, pistons, valves, and others, which worked together to facilitate air compression.

Figure 4.1 showed the compressor system driven by an electric motor. In this case, the motor transformed electrical energy into mechanical energy through a pulley system to power the load/compressor to generate pressurized air.

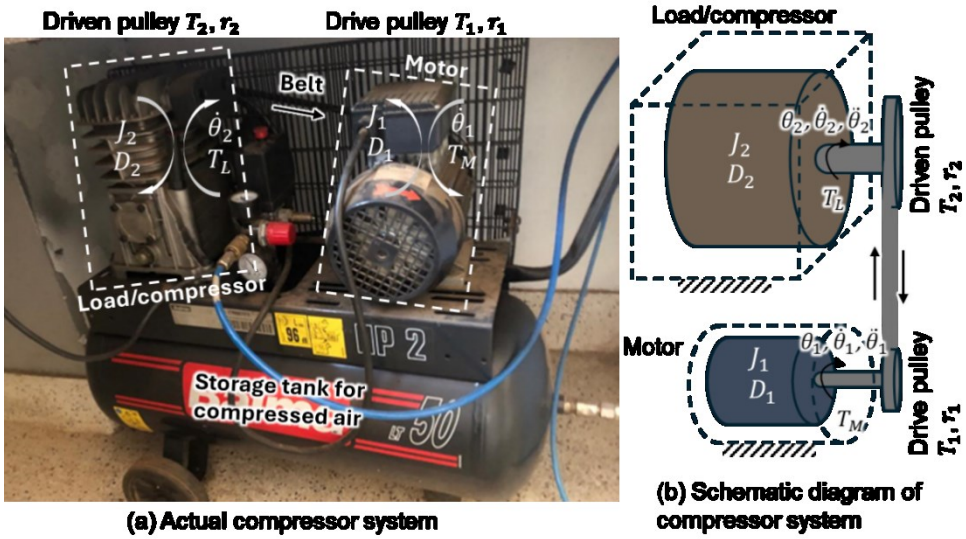


**Figure 4.1: Schematic diagram of the piston air compressor system**

The electric motor and load/compressor were designed to match electrical and mechanical requirements by evaluating parameters such as torque, speed, and friction. The dynamics of the compressor system covered the interaction between the motor and the load/compressor;

however, if not controlled, this interaction generated vibrations, disturbances, and mechanical stress within the system. The parameters shown in Figure 4.1 were defined as indicated in Table 4.1:

**Table 4.1: Description of compressor system parameters**

| Compressor Parameters | Description | Physical Meaning |
|---|---|---|
| $T_M$ | Electric Motor Torque | This was the motor-generated torque that acts as the system's input which initiated rotational motion. |
| $J_1$ | Moment of Inertia of the Electric Motor | Influenced the system's acceleration characteristics and response time. |
| $J_2$ | Moment of Inertia of the Compressor Piston | Quantified the load's resistance to changes in rotational motion |
| $\ddot{\theta}_1$ | Angular Acceleration of the electric motor | It indicated how quickly the motor's rotational speed was changing. |
| $\dot{\theta}_1$ | Angular Speed of the electric motor | State variables that defined motor motion. |
| $\theta_1$ | Angular Displacement of the Electric Motor | It helped in tracking the rotational state of the motor. |
| $\ddot{\theta}_2$ | Angular Acceleration of the load/compressor | Represented the rate at which the load's rotational speed changed over time. |
| $\dot{\theta}_2$ | Angular Speed of the load/compressor | The rate at which the load's rotational speed changed over time |
| $\theta_2$ | Angular Displacement of the load/compressor | Indicated the position of the piston in the compression cycle |
| $D_1$ | Friction or Damping Coefficient for the Electric Motor | Represented losses that determined motor deceleration without input. |
| $D_2$ | Friction or Damping Coefficient for the load/compressor | Represented resistance forces such as mechanical friction and air drag within the load system. |
| $r_1$ | Radius of the Primary Pulley | Influenced the pressure generation and work done during the piston's cycle |
| $r_2$ | Radius of the Secondary Pulley | Helped in defining the speed and torque characteristics of the load side |
| $T_L$ | Load/compressor Torque | The cyclically varying torque required for air compression. |

### 4.1.2 Mathematical Model for the Compressor System

The equation governing the motor drive system of the air compressor in Figure 4.1 was represented as a second-order control system as shown in (4.1);

$$T_M = J_1\ddot{\theta}_1 + D_1\dot{\theta}_1 + T_1 \tag{4.1}$$

The input power of the motor was used to counteract two main primary elements: the system's inertia $J_1$ and a damping effect $D_1$which hinders movement. It was important to understand that the load or compressor requires a specific amount of torque to operate effectively, which was transmitted from the secondary pulley to the primary pulley as $T_1$. It was noted that the motor had to produce sufficient torque, or rotational force, to drive the load or compressor via the pulley system. *($J_1\ddot{\theta}_1$)* - quantified the torque necessary to produce rotational acceleration in the motor whereas *($D_1\dot{\theta}_1$)* represented the energy dissipated due to frictional effects and other resistive forces within the motor, such as bearing friction and aerodynamic drag. During its operation, the motor initially overcame $J_1$ and $D_1$ to generate a force $T_1$ which was transferred to the primary pulley. This torque $T_1$, carried the additional load from the load/compressor and the fan while varying its speed.

On the load/compressor side, $T_1$ generated a force $T_2$ which counteracted the load/compressor forces; the torque needed for the load/compressor $T_L$, the inertia of the compressor side $J_2$, and its damping effect $D_2$. In essence, the motor overcame both its own resistance and that of the load/compressor, transferring force through the pulleys to drive the entire system. To this end, the compressor dynamics were given by;

$$T_2 = J_2\ddot{\theta}_2 + D_2\dot{\theta}_2 + T_L \tag{4.2}$$

($T_2$) denoted the torque applied to the load or compressor side, typically transferred from the motor through a coupling or shaft. It functioned as the driving force that initiated and maintained the rotational movement of the load. ($J_2\ddot{\theta}_2$) represented the torque required to change the rotational speed of load-side components whereas ($D_2\dot{\theta}_2$) represented the damping torque acting on the compressor load side. Its importance was to model the energy dissipated due to friction, air resistance, and other damping effects in the load/compressor

The relationship between $T_1$ , $T_2$; $r_1$ and $r_2$ was determined by considering that the linear distance traveled by both the pulleys which was the same. This implied that; $\theta_1 r_1 = \theta_2 r_2$ $So$, $\frac{\theta_2}{\theta_1} = \frac{r_1}{r_2}$ and the relationship between $\frac{\theta_2}{\theta_1}$ and $\frac{r_1}{r_2}$ could also be written in the form of angular acceleration and angular speed as;

$$\frac{\ddot{\theta_2}}{\ddot{\theta_1}} = \frac{\dot{\theta_2}}{\dot{\theta_1}} = \frac{r_1}{r_2} \tag{4.3}$$

For the compressor system utilized in this study in Figure 4.1, the pulley ratio was given by;

$$Pulley\ Ratio = \frac{Radius\ of\ Driven\ Pulley}{Radius\ of\ Driving\ Pulley} = \frac{r_1}{r_2} = \frac{1031}{1000} = 1.031 \tag{4.4}$$

This ratio played a role in controlling the output speed and torque transfer in the piston air compressor system as indicated in Figure 4.1. A ratio close to 1, such as 1.031, indicated only a slight difference in speed between the motor and the load/compressor, aiming for balanced performance while managing torque and speed efficiently.

Additionally, the transfer of power between the primary and secondary pulley assuming there was no power loss was given by;

$$T_1\dot{\theta}_1 = T_2\dot{\theta}_2 \text{ which meant that } \frac{T_1}{T_2} = \frac{\dot{\theta}_2}{\dot{\theta}_1} = \frac{r_1}{r_2} \tag{4.5}$$

Representing the relationship between $T_1$ and $T_2$.

$$T_1 = \left[\frac{r_1}{r_2}\right] T_2 \tag{4.6}$$

Substituting (4.6) in (4.2).

$$T_1 = \left[\frac{r_1}{r_2}\right] (J_2\ddot{\theta}_2 + D_2\dot{\theta}_2 + T_L) \tag{4.7}$$

By substituting (4.7) in (4.1)

$$T_M = J_1\ddot{\theta}_1 + D_1\dot{\theta}_1 + \left[\frac{r_1}{r_2}\right]\left(J_2\ddot{\theta}_2 + D_2\dot{\theta}_2 + T_L\right) \tag{4.8}$$

From (4.3), $\ddot{\theta}_2$ was made the subject

where;

$$\ddot{\theta}_2 = \frac{r_1}{r_2}\ddot{\theta}_1 \tag{4.9}$$

and $\frac{\dot{\theta_2}}{\dot{\theta_1}} = \frac{r_1}{r_2}$, such that

$$\dot{\theta}_2 = \frac{r_1}{r_2}\dot{\theta}_1 \tag{4.10}$$

Rewriting (4.8) in terms of $\theta_1$ by substituting (4.9) and (4.10) gave;

$$T_M = J_1\ddot{\theta}_1 + D_1\dot{\theta}_1 + \left[\frac{r_1}{r_2}\right](J_2\frac{r_1}{r_2}\ddot{\theta}_1 + D_2\frac{r_1}{r_2}\dot{\theta}_1 + T_L)$$

$$T_M = J_1\ddot{\theta}_1 + D_1\dot{\theta}_1 + \left[\frac{r_1}{r_2}\right]\left(J_2\frac{r_1}{r_2}\ddot{\theta}_1 + D_2\frac{r_1}{r_2}\dot{\theta}_1 + T_L\right)$$

$$T_M = \underbrace{\left(J_1 + J_2\left[\frac{r_1}{r_2}\right]^2\right)}_{J_{equiv}}\ddot{\theta}_1 + \underbrace{\left(D_1 + \left[\frac{r_1}{r_2}\right]^2 D_2\right)}_{D_{equiv}}\dot{\theta}_1 + \left[\frac{r_1}{r_2}\right]T_L \tag{4.11}$$

From (4.11), the overall mathematical equation of the compressor system was summarized as;

$$J_{equiv}\ddot{\theta}_1 + D_{equiv}\dot{\theta}_1 + \left[\frac{r_1}{r_2}\right]T_L = T_M \tag{4.12}$$

where;

$$J_{equiv} = J_1 + J_2 \left[\frac{r_1}{r_2}\right]^2 \tag{4.13}$$

$$D_{equiv} = D_1 + \left[\frac{r_1}{r_2}\right]^2 D_2 \tag{4.14}$$

The findings indicated that measuring only the motor position and torque was sufficient for system analysis, and equation (4.12) was identified as defining the first specific objective in modelling the compressor system.

### 4.1.3 Transfer Function of the Compressor System

From (4.12), the transfer function was derived as follows;

Considering the Laplace transform applied and initial conditions assumed to be zero, equation (4.12) was converted accordingly.

$$J_{equiv} s\ddot{\theta}_1(s) + D_{equiv}\dot{\theta}_1(s) + \left[\frac{r_1}{r_2}\right] T_L(s) = T_M(s) \tag{4.15}$$

where:$\dot{\theta}_1(s)$ was the Laplace transform of $\dot{\theta}_1(t)$.

Solving for $\dot{\theta}_1(s)$ by isolating $\dot{\theta}_1(s)$ was rearranged as;

$$\dot{\theta}_1(s) = \frac{T_M(s) - \left[\frac{r_1}{r_2}\right] T_L(s)}{J_{equiv} s + D_{equiv}} \tag{4.16}$$

Therefore, the transfer function $G_{equiv}$ by assuming that no external torque or $\left[\frac{r_1}{r_2}\right] T_L = 0$ and relating the motor torque $T_M(s)$ to the angular speed $\dot{\theta}_1(s)$ was represented as;

$$G_{equiv} = \frac{\dot{\theta}_1(s)}{T_M(s)} = \frac{1}{J_{equiv} s + D_{equiv}} \tag{4.17}$$

Equation (4.17) illustrated how the motor torque $T_M$ drove the load or compressor represented in the transfer function $G_{equiv}$, resulting in an output angular velocity $\dot{\theta}_1$ in the Laplace domain

(denoted by "s"). The transfer function modeled the system as first-order, where the time constant was determined by the combined effects of inertia and damping. The parameters $J_{equiv}$ (equivalent moment of inertia) and $D_{equiv}$ (equivalent damping coefficient) captured the dynamic behavior of all components within the compressor system. Specifically, $J_{equiv}$ denoted the equivalent moment of inertia, reflecting the combined resistance of the motor and load to angular acceleration. A higher value of $J_{equiv}$ indicated increased difficulty in accelerating the system, thereby requiring greater torque. On the other hand, $D_{equiv}$ represented the equivalent damping coefficient, accounting for resistive forces such as friction and aerodynamic drag that oppose motion. These parameters could be used in modelling energy dissipation in mechanisms within the system, including bearing friction and air resistance.

Considering (4.13) and (4.14), $r_1$ and $r_2$ were known from the specifications of the compressor system as shown in (4.4). Therefore, the next step involved determination of the values of parameters $J_1$, $D_1$, $J_2$, and $D_2$.

### 4.1.4 Determination of Inertia, and Damping Terms of the Motor Side Dynamics

The motor inertia $J_1$ and damping coefficient $D_1$ were determined by considering the electric motor circuit as indicated in Figure 4.2.

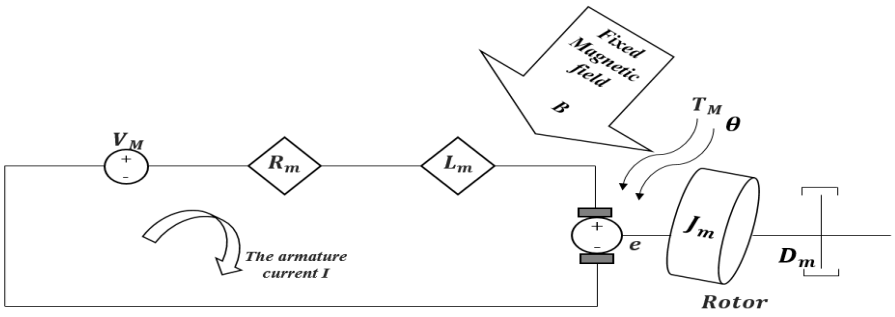


**Figure 4. 2: Uni-electric motor circuit**

Figure 4.2 consisted of the magnetic field $B$ produced by the permanent magnet rotor which was spinning. The current produced by the stator windings was made to rotate at a rotor speed by the action of a control system. When the armature current moved through a magnetic field, it produced a force.

$$\vec{F} = \vec{I}.\vec{B} \tag{4.18}$$

where; $\vec{I}$ was the armature current vector whereas $\vec{B}$ was the magnetic field

There were two approaches which controlled the strength of force that was affected by the current and magnetic field. The first approach was the armature control which involved changing the torque by changing the current in the rotor. The second approach was the field control which involved changing the torque by changing the strength of the magnetic field.

From Figure 4.2, the rotor spined with a rotational inertia $J_m$ with a damping coefficient $D_m$. Applying Lorentz's Law, the force $F_m$ generated on the rotor was equal to the function of current through the armature and the strength of the magnetic field as represented in (4.18). The motor torque $T_M$ generated by this force acted on the rotor windings at a distance/radius $r_m$ from the center of rotation, following the (4.19) as indicated:

$$T_M = F_m r_m \tag{4.19}$$

By comparing (4.19) with (4.20), $K_m$ replaced the variable $r_m$. As the rotor rotated, the direction of the force $\vec{F}$ changed with the alternating magnetic field. From (4.18), substituting for $F_m$.with $BI$ and coming up with (4.20) as indicated.

$$T_M = K_m BI \tag{4.20}$$

where $K_m$ was based on the geometry of the position of the coils relative to the magnetic field $B$. Since the armature-controlled approach was used, the magnetic field was considered a constant. Therefore, combining $K_m$ and $B$ gave the motor torque constant $K\left(\frac{\mathrm{Nm}}{\mathrm{A}}\right)$.

The motor torque was proportional to the armature current with some proportionality constant $K$ which depended on the geometry $K_m$ and strength of magnetic field was represented as;

$$T_M = KBI \tag{4.21}$$

Assuming that the magnetic field $B$ was constant, and that $T_M$ was proportional to only the armature current, this was expressed as.

$$T_M = KI \tag{4.22}$$

Based on Faraday's Law, that the back e.m.f $(e)$ is proportional to the angular speed of the motor shaft with proportionality constant factor $(K_{AV})$ expressed in volts per radian per second (V·s/rad) as shown in (4.23);

$$e = \frac{d\theta_1}{dt} K_{AV} \tag{4.23}$$

The current induced in the conductor through a coil moved through the magnetic field to produce an e.m.f which was proportional to how fast the rotor was spinning denoted by $\frac{d\theta_1}{dt}$. The e.m.f induced moved in an opposite direction to the externally applied voltage $V_M$. In this context, $K_{AV}$ was referred to as the back e.m.f. constant. When the units of $K_m$ and $K_{AV}$ were consistent, the motor constant and the back e.m.f. constant became equal, expressed as $K_m = K_{AV} = K$, from which the model representing the electrical and mechanical domains was derived.

**Electrical Domain**

Applying Kirchhoff's voltage (loop) law and referring to Figure 4.2, the input voltage equation was derived as follows:

$$V_M - R_m L_m - L_m \frac{dI}{dt} - e = 0 \tag{4.24}$$

As the circuit was traversed, the voltage source was encountered first, and upon reaching the resistor, the voltage dropped in accordance with Ohm's law, proportional to the product of the current through the resistor. A voltage was then observed across the inductor, where the drop was proportional to the rate of change of current, $\frac{dI}{dt}$. Subsequently, a voltage drop occurred across the rotor due to the back e.m.f. ($e$). Since voltage represented the potential difference around the circuit, the difference between a point and the same point was equal to zero.

**Mechanical Domain**

Applying Newton's Law, the sum of moments was equal to the inertia

$$\sum M = J \propto \tag{4.25}$$

A torque acting on the inertia was generated by the motor and there was a resistant torque due to friction. By modelling the friction, friction was equated to the speed of the motor or the speed at which the rotor was rotating/spinning as shown in (4.26).

$$T_M - D_m \dot{\theta}_1 = J_m \ddot{\theta}_1 \tag{4.26}$$

where; $T_M - D_m \dot{\theta}_1$ was the sum of moments and $J_m$ was the rotor inertia.

By combining the (4.24) and (4.26), the relationship between the input voltage $V_M$ and the motor's output speed $\dot{\theta}_1$ was determined through the use of the open loop transfer function.

Applying the Laplace transform, (4.24) and (4.26) were expressed in terms of the Laplace variable '*s*', assuming zero initial conditions.

$$V_M(s) - R_m L_m(s) - L_m I(s) - K D_m \dot{\theta}_1(s) = 0 \tag{4.27}$$

$$K_m I(s) - D_m s\dot{\theta}_1\,(s) = J_m s^2 \dot{\theta}_1(s) \tag{4.28}$$

Arriving at the open-loop transfer function, *I*(*s*) was eliminated from (4.27) and (4.28); where the rotational speed $\dot{\theta}_1$ was considered the output and the armature voltage $V_M$ was considered the input.

$$I(s) = \frac{J_m s^2 + D_m s}{K_m} \tag{4.29}$$

By substituting (4.29) into (4.27) gave;

$$\frac{\dot{\theta}_1(s)}{V_M(s)} = \frac{K_m}{(J_m s + D_m)(L_m s + R_m) + K^2} \left[\frac{rad/sec}{V}\right]$$

$$\frac{\dot{\theta}_1(s)}{V_M(s)} = \frac{K_m}{J_m L_m s^2 + (J_m R_m + D_m L_m) s + D_m R_m + {K_m}^2} \left[\frac{rad/sec}{V}\right] \tag{4.30}$$

From (4.30),

$$J_1 = L_m J_m \tag{4.31}$$

$$D_1 = J_m R_m + D_m L_m \tag{4.32}$$

Considering the specifications of the compressor system in Table 4.2,

**Table 4.2: Specifications of the Compressor System**

| Description | Value Specifications | Source of information |
|---|---|---|
| Power | 1.25 kW | Manufacturer datasheet (e.g., UniElectric M80-2M or similar IEC motors)<br>- *IEC 60034* and *NEMA MG 1* standards for electric motor design |
| Voltage | 230 V | Manufacturer datasheet (e.g., UniElectric M80-2M or similar IEC motors)<br>- *IEC 60034* and *NEMA MG 1* standards for electric motor design |
| Frequency | 50 Hz | Manufacturer datasheet (e.g., UniElectric M80-2M or similar IEC motors)<br>- *IEC 60034* and *NEMA MG 1* standards for electric motor design |
| Permanent magnet/rotor flux linkage | 0.14 H | Manufacturer datasheet (e.g., UniElectric M80-2M or similar IEC motors)<br>- *IEC 60034* and *NEMA MG 1* standards for electric motor design |
| Number of Motor Poles ($\boldsymbol{P}$) | 2 | Manufacturer datasheet (e.g., UniElectric M80-2M or similar IEC motors)<br>- *IEC 60034* and *NEMA MG 1* standards for electric motor design |
| Moment of Inertia of the rotor ($\boldsymbol{J_m}$) | $3.2284 \times 10^{-6}$ kg·m² | *Krause, P. C., Wasynczuk, O., & Sudhoff, S. D. (2002).* "Analysis of Electric Machinery and Drive Systems", Wiley. |
| Speed (no-load speed) | 2750 rpm | Manufacturer datasheet (e.g., UniElectric M80-2M or similar IEC motors)<br>- *IEC 60034* and *NEMA MG 1* standards for electric motor design |
| Full Load Amps | 8.3 amps | Manufacturer datasheet (e.g., UniElectric M80-2M or similar IEC motors)<br>- *IEC 60034* and *NEMA MG 1* standards for electric motor design |
| Damping coefficient ($\boldsymbol{D_m}$) | $3.5077 \times 10^{-6}$ Nm/s | *Ogata, K.* (2010). "Modern Control Engineering", Prentice Hall – mechanical modeling sections. |
| Rotor Resistance ($\boldsymbol{R_m}$) | 4 Ω | *Gieras, J. F., & Wing, M.* (2002). "Permanent Magnet Motor Technology", CRC Press. |
| Keyed Shaft Diameter | 3/4 inch | Manufacturer datasheet (e.g., UniElectric M80-2M or similar IEC motors)<br>- *IEC 60034* and *NEMA MG 1* standards for electric motor design |
| Frame Size | 80 (specifically, 90L frame size) | Manufacturer datasheet (e.g., UniElectric M80-2M or similar IEC motors)<br>- *IEC 60034* and *NEMA MG 1* standards for electric motor design |

By referring to the (4.13) and (4.14) given that the pulley ratio was known from (4.4), the values of $J_1, and\ D_1$ were determined by calculating the inductive reactance. Considering the motor frequency (single-phase type), the inductive reactance $X_L$ was expressed as:

$$X_L = 2\pi f L_m \tag{4.33}$$

where; $X_L$ was the inductive reactance estimated from current, voltage, $f$ was the frequency and $L_m$ was the inductance.

The inductive reactance was estimated from the difference between the total impedance $Z$ and the resistance as:

$$Z = \frac{V}{I} = \frac{230}{8.3} = 27.7\Omega \tag{4.34}$$

And $X_L = \sqrt{Z^2 - R_m{}^2} = \sqrt{(27.7^2 - 4^2)} = 27.99$

Therefore;

$$X_L = 2\pi f L_m\ but\ L_m\ = \frac{X_L}{2\pi f} = \frac{27.99}{2\pi x50} = 0.09H \tag{4.35}$$

Substituting (4.35) into (4.31) gives;

$$J_1 = L_m J_m = (0.09x3.2284x10^{-6}) = 2.96x10^{-7}\text{kg} \cdot \text{m}^2$$

From (4.32) the values of $D_1$ were determined as;

$D_1 = J_m R_m + D_m L_m = (3.2284x10^{-6}x4) + (3.5077x10^{-6}x0.09) = 1.323x10^{-5}$ Nm/s

### 4.1.5 Determination of the Moment of Inertia $J_2$ and the Damping Coefficient $D_2$ of Compressor Side Dynamics

The compressor moment of inertia $J_2$ and the damping coefficient were determined through the following steps. According to Mu-jun & Jian, (2010) the compressor system was commonly

used in practical applications; however, obtaining an accurate model was difficult. The investigation also indicated that, by considering the characteristics of the air compressor system, it could be divided into a pressure-rising process and a constant-pressure process. In this case, the pressure-rising process resembled a first-order inertia system with a large time constant $t_1$, while the constant-pressure process represented a pure delay system, where the pressure was considered essentially unchanged. In addition, the speed control system based on vector control and a synchronous motor could be approximately represented as a first-order inertia system with time constant $t_2$, as presented in equation (4.36).

$$G(s) = \frac{K_c\, e^{-\tau s}}{(t_1 s+1)(t_2 s+1)} \tag{4.36}$$

where; $K_c$ as the proportionality factor of the system, $t_1$ as the inertia time constant, $t_2$ as the equivalent time constant for the speed control system, $e^{-\tau s}$ as the time delay in the system, which did not affect the order of the system but added a delay to the response.

Note: By ignoring the time delay in the system, (4.36) was reduced to;

$$G(s) = \frac{K_c}{(t_1 s+1)(t_2 s+1)} \tag{4.37}$$

Applying partial fractions,

$$\frac{K_c}{(t_1 s+1)(t_2 s+1)} = \frac{P}{(t_1 s+1)} + \frac{Q}{(t_2 s+1)} \quad \ldots\ldots \tag{4.38}$$

$$K_c = P(t_2 s + 1) + Q(t_1 s + 1) \tag{4.39}$$

Constants: $K_c = P + Q$

Comparing coefficients of ‘s’ resulted into;

$s$: $0 = Pt_2 + Qt_1$; so, $P = \frac{-Qt_1}{t_2}$

$$K_c = Q - \frac{Qt_1}{t_2} \text{ or } \frac{Q(t_2 - t_1)}{t_2}$$

$$Q = \frac{K_c\, t_2}{t_2 - t_1} \text{ and } P = \frac{-K_c t_2 t_1}{t_2(t_2 - t_1)}$$

Therefore,

$$G(s) = \frac{K_c}{(t_1 s+1)(t_2 s+1)} = \underbrace{\frac{\frac{-K_c t_2 t_1}{t_2(t_2 - t_1)}}{t_1 s+1}}_{\text{Rising Pressure}} + \underbrace{\frac{\frac{K_c t_2}{(t_2 - t_1)}}{(t_2 s+1)}}_{\text{Constant Pressure}} \tag{4.40}$$

From (4.40), the focus was on maintaining a constant pressure, as the piston compressor was intended to operate under stable pressure conditions.

$G(s) = \frac{\frac{K_c t_2}{(t_2 - t_1)}}{t_2 s+1}$, by dividing through with the numerator $\frac{K_c t_2}{(t_2 - t_1)}$, (4.40) was written as a first order system as shown in (4.41).

$$G(s) = \frac{1}{\left(\frac{t_2 - t_1}{K_c}\right)s + \frac{t_2 - t_1}{K_c t_2}} \tag{4.41}$$

From (4.41), assuming $J_2 = \frac{t_2 - t_1}{K_c}$ (4.42)

where as $D_2 = \frac{t_2 - t_1}{K_c\, t_2}$ (4.43)

Referring to (4.13) and (4.14); $J_{equiv}$ and $D_{equiv}$ were determined as follows;

$$J_{equiv} = J_1 + J_2 \left[\frac{r_1}{r_2}\right]^2 = 2.96\text{x}10^{-7} + 0.1[\,1.031]^2 = 0.1063$$

$$D_{equiv} = D_1 + \left[\frac{r_1}{r_2}\right]^2 D_2 = 1.323\text{x}10^{-5} + 0.2222\text{x}[\,1.031]^2 = 0.2362$$

### 4.1.6 Determination of $t_1$ and $t_2$

From (4.41), assuming that $J_G = \frac{t_2 - t_1}{K_c}$

(4.44)

and $D_G \frac{t_2 - t_1}{K_c t_2}$

(4.45)

The first Ordinary Differential Equation (ODE) was described by the standard form given by;

$$G(s) = \frac{1}{J_G s + D_G} = \frac{\frac{1}{D_G}}{\frac{J_G}{D_G} s + \frac{D_G}{D_G}}$$

which was written in form of;

$$G(s) = \frac{K_G}{\tau s + 1} \tag{4.46}$$

$$K_G = \frac{K_c t_2}{t_2 - t_1} \tag{4.47}$$

$$\tau = \frac{\frac{t_2 - t_1}{K_c}}{\frac{t_2 - t_1}{K_c t_2}} = t_2 \tag{4.48}$$

Considering a first order system,

The Step Response $u(t) = 1(t)$

The Laplace Transform of a unit step $1(t) = \frac{1}{s} = U(s)$

The input was $U(s)$ and output it was denoted by $Y(s)$

$$\mathrm{G(s)} = \frac{\mathrm{Y(s)}}{\mathrm{U(s)}} = \frac{\mathrm{K_G}}{\tau \mathrm{s} + 1} \tag{4.49}$$

Then, $\mathrm{Y(s)} = \mathrm{U(s)G(s)} = \frac{\mathrm{K_G}}{\tau s+1}\mathrm{x}\frac{1}{\mathrm{s}}$

Rearranging by splitting $\frac{\mathrm{K_G}}{\tau s+1}\mathrm{x}\frac{1}{\mathrm{s}}$;

Using partial fractions.

$$\frac{\mathrm{K_G}}{\tau s+1}\mathrm{x}\frac{1}{\mathrm{s}} = \frac{\mathfrak{y}}{\mathrm{s}} + \frac{\mathrm{W}}{\tau s+1} = \frac{\mathfrak{y}(\tau s+1)+\mathrm{W}s}{\mathrm{s}(\tau s+1)} \tag{4.50}$$

By solving for $\mathfrak{y}$ and W,

In matching or comparing numerators;

$'s'$ terms:

On the left $s = 0$ while on the right $\mathfrak{y}\tau + \mathrm{W}$

$'s^0'$ terms

On the left side of (4.50),

$$\mathrm{K_G} = \mathfrak{y} \tag{4.51}$$

while the right was equated to zero.

So, $\mathfrak{y}\tau + \mathrm{W} = 0$, where; $\mathrm{W} = -\mathfrak{y}\tau$ or $-\mathrm{K_G}\tau$ (4.52)

$$\frac{\mathfrak{y}}{\mathrm{s}}\mathrm{x}\frac{\mathrm{W}}{\tau s+1} = \left[\frac{\mathrm{K_G}}{\mathrm{s}} - \frac{\mathrm{K_G}\tau}{(\tau s+1)}\right] \tag{4.53}$$

Finding the inverse transform of (4.53),

$$y(t) = \mathcal{L}^{-1}[Y(s)] = \mathcal{L}^{-1}\left[\frac{K_G}{s} - \frac{K_G\tau}{\tau s+1}\right] \tag{4.54}$$

Dividing (4.54) by $\tau$ gave;

$$y(t) = \mathcal{L}^{-1}\left[\frac{K_G}{s} - \frac{K_G}{\left(s+\frac{1}{\tau}\right)}\right] = K_G - K_G e^{\frac{-t}{\tau}} = K_G\left(1 - e^{\frac{-t}{\tau}}\right) \tag{4.55}$$

$x_p$ = Real part and $x_n$ as the Imaginary part or response of the system. Considering a step response, $y(t) = K_G\left(1 - e^{\frac{-t}{\tau}}\right), at\ t \geq 0$

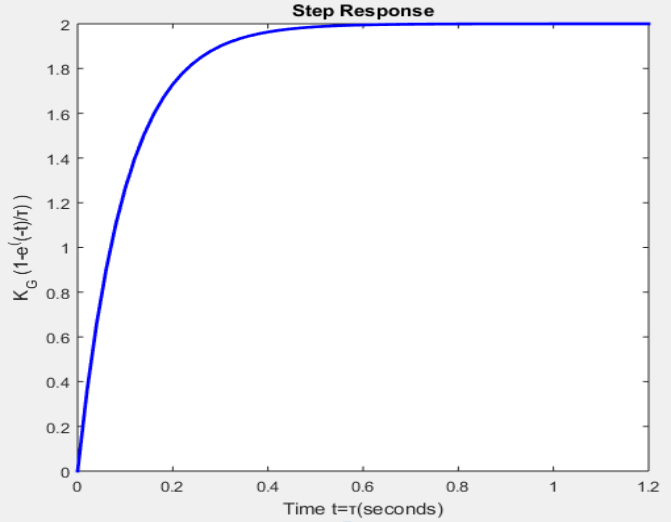


**Figure 4. 3: Step response "y(t)" of a dynamic system**

From the above Figure 4.3, Given that $t = \tau = 0.5$ seconds when $K_G = 2$

$$y(t) = K_G\left(1 - e^{\frac{-t}{\tau}}\right) = 1.2642$$

For $t = 0.3$, $K_G = 1.8$ Therefore;

$$y(t) = K_G\left(1 - e^{\frac{-t}{\tau}}\right) = 1.1378$$

From the rule of thumb, once the output reached 2% of the final value, it was considered that the system was in its steady state.

So, $t_1 = 0.3$ and $t_2 = 0.5$; By substituting in;

$$G(s) = \frac{K_G}{(t_1 s+1)(t_2 s+1)} = \frac{1}{(0.3s+1)(0.5s+1)} \quad (4.56)$$

$$J_2 = \frac{t_2 - t_1}{K_G} = \left(\frac{0.5-0.3}{2}\right) = 0.1 \quad (4.57)$$

$$D_2 = \frac{t_2 - t_1}{K_G t_2} = \left(\frac{0.5-0.3}{1.8\text{x}0.5}\right) = 0.2222 \quad (4.58)$$

## 4.2 Control System Design

The goal of this section was to design a control system that regulated the dynamic behavior of the air compressor, based on the derived transfer function model in Equation (4.11).

### 4.2.1 Uncontrolled Compressor System

The block diagram representing an uncontrolled compressor system is shown in Figure 4.4

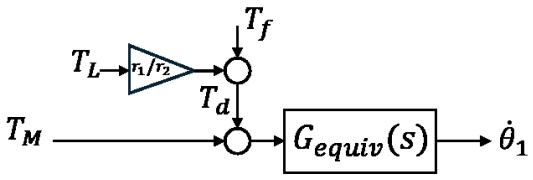


**Figure 4. 4: Uncontrolled compressor system**

Figure 4.4 represents the uncontrolled compressor with an input torque $T_M$ from the electric motor which runs the air compressor system/plant**.** $T_d$ is the external disturbance force characterized by friction and vibrations into the system which comprises the load/compressor torque $T_L$.

Note: Friction in the motor is introduced in Figure 4.4 as $T_f$ such that;

$$T_d(s) = \left(\frac{r_1}{r_2}\right) T_L(s) + T_f(s) \quad (4.59)$$

In the next sections, the control system is designed to enhance the tracking performance and suppress the effects of the disturbances, $T_d$.

### 4.2.2 Design of the Feedback Controller

To enhance tracking performance, a PID Controller was introduced as shown in Figure 4.5.

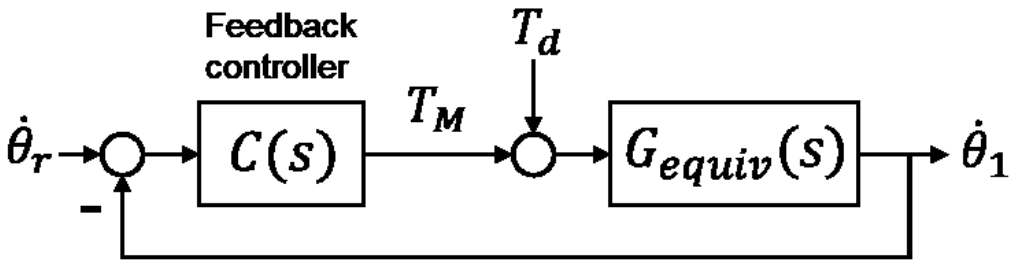


**Figure 4.5:Design of the feedback controller**

where, $\dot{\theta}_r$ as the desired/speed reference, $C$ as the controller which was designed as a PID in this study given as,

$$C(s) = K_p + K_D s + \frac{K_I}{s} \tag{4.60}$$

where $K_p$, $K_D$ and $K_I$ were proportional derivatives and integral gains

Introducing a PID $(C)$ feedback loop of Figure 4.5 above resulted in an improved and accurate system. This was because there was continuous monitoring of the output and adjustment of the inputs which produced a high precision in the desired system performance. The closed-loop system stabilized the system especially in the presence of external disturbances. Ultimately, continuous feedback allowed for performance improvements, as the system learned and adapted based on previous performance.

From Figure 4.5,

$$\dot{\theta}_1(s) = G_{equiv}(s)T_d(s) + G_{equiv}(s)C(s)[\dot{\theta}_r(s) - \dot{\theta}_1(s)] \tag{4.61}$$

Beyond equation (4.61), the Laplace operator $(s)$ was ignored for simplicity.

$$\dot{\theta}_1 = G_{equiv}T_d + G_{equiv}C\dot{\theta}_r - G_{equiv}C\dot{\theta}_1$$

$$\left(1 + G_{equiv}C\right)\dot{\theta}_1 = G_{equiv}T_d + G_{equiv}C\dot{\theta}_r$$

$$\dot{\theta}_1 = \frac{G_{equiv}}{\left(1 + G_{equiv}C\right)} T_d + \frac{G_{equiv}C}{\left(1 + G_{equiv}C\right)} \dot{\theta}_r$$

where $\frac{G_{equiv}C}{(1+G_{equiv}C)}$ was the reference tracking part and $\frac{G_{equiv}}{(1+G_{equiv}C)}$ was the disturbance rejection part.

$$\dot{\theta}_1 = \left(\frac{G_{equiv}C}{1+G_{equiv}C}\right) \dot{\theta}_r + \left(\frac{G_{equiv}}{1+G_{equiv}C}\right) T_d \tag{4.62}$$

If the PID controller $C$ in (4.61) was well designed, the reference performance could be enhanced as shown in (Samuel, 2023, Samuel et al., 2021)

In addition, the effects of disturbances were reduced by increasing the controller proportional gain, $K_p$. However, considering the operating conditions of the compressor system in Figure 2.1, $K_p$ was not sufficient enough to suppress the effects of the large disturbances such as excessive vibrations. On the other hand, a disturbance observer was been proven to reject such extreme disturbances (Samuel, 2023, Samuel et al., 2024).

### 4.2.3 Proposed Disturbance Observer-Based (DOB) Control System

A disturbance observer (DOB) was introduced to robustly mitigate disturbances, enhancing the efficiency of motion control systems (Samuel, Haninger, Oboe, & Oh, 2024). For instance, when introduced in the system, a disturbance observer further improved its performance by suppressing the effects of vibration as indicated in Figure 4.6. Additionally, it enhanced robustification to parameter variations. The disturbance observer was defined by three parameters: the compensation gain, the observer's cut-off frequency, and the moment of inertia used in the observer (K. Samuel & Oh, 2022). It was pointed out that, by appropriately selecting these parameters, vibration could be effectively suppressed in the second order-inertia system. To this end, the DOB was designed for Figure 4.5 and the revised block diagram was presented in Figure 4.6.

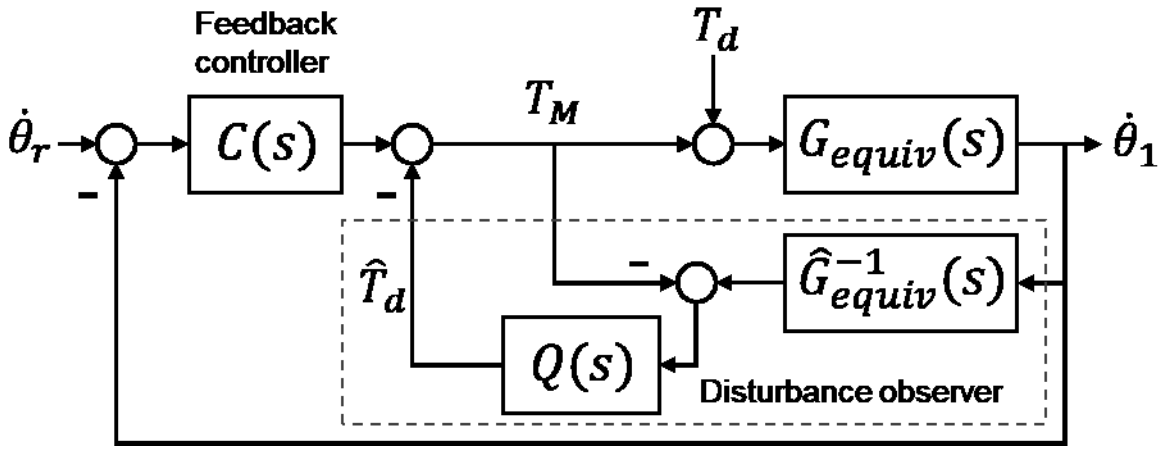


**Figure 4. 6: Proposed control architecture of a DOB**

where $\hat{G}_{equiv}\ (s)$ as the nominal mode of $G_{equiv}(s)$ and $Q(s)$ as the $Q$-filter.

These were designed as;

$$\hat{G}_{equiv}(s) = \frac{1}{\hat{J}_{equiv}\,(s)+\hat{D}_{equiv}} \tag{4.63}$$

$$Q(s) = \frac{\omega_Q}{s+\omega_Q} \tag{4.64}$$

Where $\hat{J}_{equiv}$ and $\hat{D}_{equiv}$ were the nominal parameters of $J_{equiv}$ and $D_{equiv}$ respectively while $\omega_Q$ was the $Q$-filter cut-off frequency. The cutoff frequency $\omega_Q$ significantly influenced the responsiveness of the Disturbance Observer (DOB) to external disruptions. A higher value allowed for quicker adaptation to system variations; however, it would also introduce high-frequency noise into the control loop, potentially affecting performance. In contrast, a lower cutoff frequency slowed down the observer's reaction but enhanced its ability to suppress noise and tolerate modeling uncertainties. As such, selecting an appropriate $\omega_Q$ involved a careful compromise between achieving rapid disturbance compensation and maintaining robustness and stability in the system. Specifically, the cutoff frequency was chosen to balance fast response to vibration disturbances, enhance noise rejection and system stability.

Subsequently, analyzing the tracking performance and disturbance rejection capabilities of the proposed method from Figure 4.6 was implemented. The function of the DOB in figure 4.6 was to estimate the disturbances $T_d$ as $\hat{T}_d$ and compensate for them in a feed-forward manner. To this end,

$$\hat{T}_d = -Q(\hat{G}_{equiv}{}^{-1}\dot{\theta}_1 - T_M) \tag{4.65}$$

$$\dot{\theta}_1 = G_{equiv}(T_d + T_M) \tag{4.66}$$

$$T_M = \hat{T}_d + C(\dot{\theta}_r - \dot{\theta}_1) \tag{4.67}$$

Substituting (4.65) into (4.67) provided;

$$T_M = C\left(\dot{\theta}_r - \dot{\theta}_1\right) - Q(\hat{G}_{equiv}{}^{-1}\dot{\theta}_1 - T_M) \tag{4.68}$$

Such that,

$$T_M = \frac{C(\dot{\theta}_r - \dot{\theta}_1) - Q\hat{G}_{equiv}{}^{-1}\dot{\theta}_1}{1-Q} \tag{4.69}$$

Substituting (4.68) into (4.66)

$$\dot{\theta}_1 = G_{equiv}T_d + \left(\frac{G_{equiv}(C(\dot{\theta}_r - \dot{\theta}_1) - Q\hat{G}_{equiv}{}^{-1}\dot{\theta}_1)}{1-Q}\right)$$

$$\dot{\theta}_1(1-Q) = (1-Q)G_{equiv}T_d + G_{equiv}C\dot{\theta}_r - G_{equiv}C\dot{\theta}_1$$

$$- G_{equiv}Q\hat{G}_{equiv}{}^{-1}\dot{\theta}_1$$

$$\left(1 - Q + G_{equiv}C + G_{equiv}Q\hat{G}_{equiv}{}^{-1}\right)\dot{\theta}_1 = (1-Q)G_{equiv}T_d + G_{equiv}C\dot{\theta}_r$$

$$\dot{\theta}_1 = \underbrace{\frac{G_{equiv}C}{(1-Q+G_{equiv}C+G_{equiv}Q\hat{G}_{equiv}{}^{-1})}\dot{\theta}_r}_{\text{Reference tracking}} + \underbrace{\frac{(1-Q)G_{equiv}}{(1-Q+G_{equiv}C+G_{equiv}Q\hat{G}_{equiv}{}^{-1})}T_d}_{\text{Disturbance Rejection}} \tag{4.70}$$

Consider high value of $\omega_Q$ such that $Q = 1$, this is desirable for a faster response and disturbance rejection. By setting $Q = 1$ in (4.70) gives,

$$\dot{\theta}_1 = \frac{G_{equiv}C}{G_{equiv}C + G_{equiv}\hat{G}_{equiv}^{-1}}\dot{\theta}_r + 0 \tag{4.71}$$

Therefore, the disturbances were rejected. Furthermore, assuming that $\hat{G}_{equiv}^{-1}$ was properly estimated such that $\hat{G}_{equiv} = G_{equiv}$ in (4.71) became

$$\dot{\theta}_1 = \frac{G_{equiv}C}{G_{equiv}C+1}\dot{\theta}_r \tag{4.72}$$

Equation (4.72) was similar to (4.62) and reference tracking was achieved by increasing the gain $K_p$. In summary, the proposed DOB-Based Control was able to suppress the effects of disturbances as shown in (4.71). Moreover, tracking performance was equally improved.

### 4.3 Simulation Study

This section presented a validation of the developed control system's performance through simulations. Performance was evaluated based on two main criteria: the system's capability to suppress vibrations effectively and its accuracy in tracking reference signals.

#### 4.3.1 Simulation Protocol

The block diagrams shown in Figures 4.5 and 4.6 were implemented in Simulink, where a step signal with a magnitude of 1 served as the desired speed for $\dot{\theta}_r$ both configurations. The complete Simulink block diagram was provided in **Appendix B**.

#### 4.3.2 Simulation Results

The $J_{equiv}$ and $D_{equiv}$ were given in (4.13) and (4.14) $\hat{J}_{equiv}$ , $\widehat{D}_{equiv}$ $\omega_Q$ were tuned empirically in Simulink while $K_p$, $K_D$ and $K_I$ were adjusted in each of the method using a PID Tuner in Simulink. The values of all these parameters were given in the Table 4.3.

**Table 4.3: Parameter Values**

| Parameter | Value (Units) | Parameter | Values (Units) |
|---|---|---|---|
| $\boldsymbol{J_{equiv}}$ | 0.1063 | $K_p$ (No DOB) | 1.2039 |
| $\boldsymbol{D_{equiv}}$ | 0.2362 | $K_D$ (No DOB) | 0.0167 |
| | | $K_I$ (No DOB) | 6.2595 |
| $\boldsymbol{\hat{J}_{equiv}}$ | 0.04252 | $K_p$ (With DOB) | 3.3176 |
| $\boldsymbol{\hat{D}_{equiv}}$ | 0.2362 | $K_D$ (With DOB) | 0.02096 |
| | | $K_I$ (With DOB) | 28.3885 |
| $\boldsymbol{\omega_Q}$ | 30Hz | | |

The table presented a comparison of key system parameters and PID controller gains for two configurations: one without a Disturbance Observer (DOB) and one with it. The analysis included the equivalent moment of inertia and damping, PID gains-proportional $K_p$ derivative $K_D$ and integral $K_I$ as well as the DOB's cut-off frequency, denoted by $\boldsymbol{\omega_Q}$. The equivalent system parameter proved that the estimated inertia ($\boldsymbol{J_{equiv}}$ ) was lower when the DOB was incorporated, indicating its effectiveness in compensating for external disturbances and model inaccuracies. This reduction in perceived inertia enhanced the system's responsiveness and control precision.

The damping value for ($\boldsymbol{D_{equiv}}$) remained unchanged in both configurations, suggesting that the DOB primarily affected the system's inertia while the damping characteristics stayed consistent. The PID Controller Gains (*Without DOB)* suggested a conservative tuning approach aimed at maintaining system stability in the absence of disturbance compensation. However, this also resulted in slower dynamic response and limited vibration control. On the other hand,

The PID Controller Gains (*With DOB)* with substantially higher gains indicated a more assertive controller enabled by the DOB. The improved disturbance estimation allowed for a more

responsive and effective control strategy, leading to faster system response, stronger disturbance rejection, and enhanced vibration suppression.

Additionally, the DOB filter was assigned a cut-off frequency of 30 Hz, balancing noise sensitivity and responsiveness. This selection contributed to improved disturbance rejection without amplifying high-frequency noise.

Graph 1. Results for No Periodic Disturbance Added

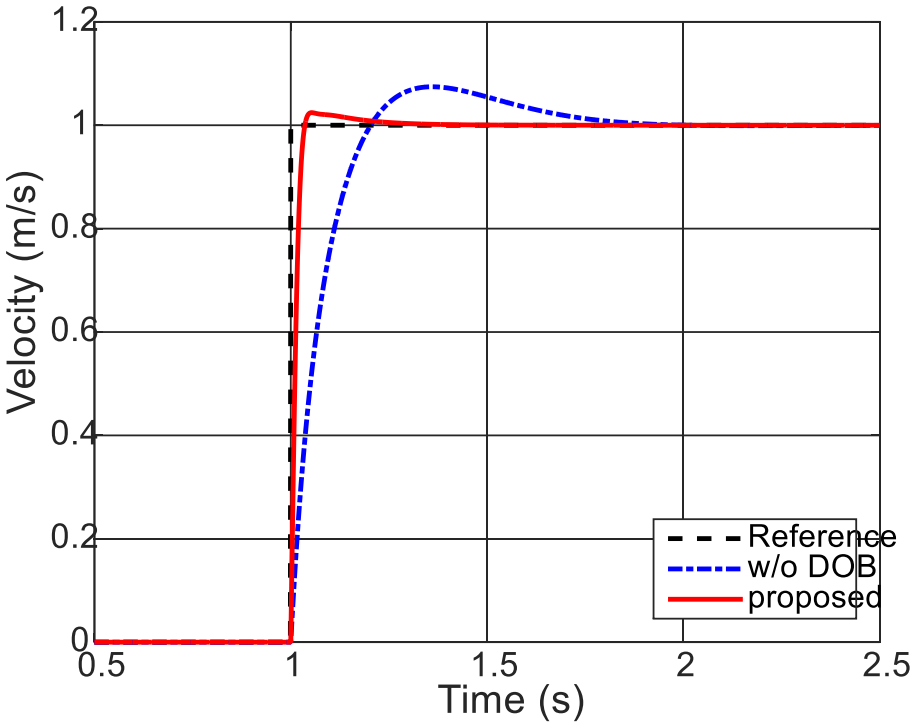


**Figure 4.7: System with no periodic disturbance added**

Figure 4.7 was used to illustrate a comparative analysis of the velocity responses for three system configurations over a duration of 2.5 seconds. The black dashed line was identified as the reference or target velocity, representing a step input that reaches 1 m/s within the first second and remains constant thereafter. The configuration without the Disturbance Observer (DOB), depicted by the blue dashed-dot line, was reported to have demonstrated a significant

overshoot beyond the desired velocity. Following this overshoot, the response was noted to exhibit a relatively slow settling time, stabilizing around 1 m/s after approximately 2 seconds.

It was indicated that this overshoot could be linked to the higher controller gains particularly the proportional and integral terms as detailed in Table 4.3. These gains had been increased to improve the system's responsiveness and enhance its ability to reject disturbances. However, this tuning approach was found to result in an underdamped behaviour, commonly associated with transient overshoot.

Additionally, it was observed that while the DOB enhanced the controller's responsiveness by increasing its sensitivity to disturbances and accelerating corrective actions, this could cause the control effort to temporarily overcompensate during abrupt changes. The derivative gain, being relatively small in this configuration, was also thought to contribute to the overshoot, as it provided insufficient damping to counter fast error variations.

In contrast, the proposed control strategy, shown by the solid red line, was reported to have achieved close tracking of the reference velocity with minimal overshoot and rapid convergence. This performance was interpreted as evidence of improved control accuracy. The DOB-based controller was thus recognized as superior to the non-DOB configuration, not only by reducing overshoot but also by ensuring quicker alignment with the target velocity.

Furthermore, it was emphasized that the system lacking DOB appeared more susceptible to disturbances, resulting in degraded tracking performance and extended settling times. The proposed controller, on the other hand, was credited with eliminating transient oscillations and adapting swiftly to system variations, reflecting its robustness.

In conclusion, these findings supported the effectiveness of the DOB-enhanced control approach for applications demanding high precision and disturbance rejection, such as in air compressors and industrial drive systems.

**Table 4. 4: Results for system with no disturbance added**

| System of measurement | Reference | w/o DOB (Blue) | Proposed (Red) | Practical Implication |
|---|---|---|---|---|
| **Rise Time (s)** | 0 | 0.20 | 0.05 | • Responded faster to commands.<br>• Worked better with changing loads. |
| **Overshoot (%)** | 0 | 8% | 2% | • Caused fewer pressure surges, reducing stress on parts.<br>• Minimized damage to valves and seals.<br>• 75% lower overshoot decreased pressure spikes.<br>• Parts lasted 20–30% longer. |
| **Settling Time (s)** | 0 | 0.70 | 0.15 | • Improved disturbance recovery enhanced vibration damping, reduced mechanical wear, and increased energy efficiency. |
| **Steady-State Error** | 0 | 0.02 | 0.01 | • Precise pressure regulation.<br>• Supported tight-tolerance applications (e.g., pneumatic tools).<br>• Minimized air wastage.<br>• Enhanced overall process quality. |

The results from Table 4.4 indicated that the proposed controller was able to attain precise velocity tracking and robust disturbance rejection. When the overshoot and settling time were reduced, the proposed controller ensured better system stability and performance which made it a reliable solution for applications requiring high system accuracy and quick adaptation to changing operating conditions.

### 4.3.3 Design of Disturbance Signals ($T_d$)

The signal builder in Figure 4.7 generated input signals that acted as external disturbances to the system, representing the presence of vibrations. The introduced wave input signals produced alternating variations to which the system had to respond.

Two cases of $T_d$ were considered.

1) **Square Wave:** This was chosen because it represented both low and high frequency characteristics of vibration. It was designed with a frequency of 0.5Hz and amplitude of 1 in 3 seconds as shown in Figure 4.8.

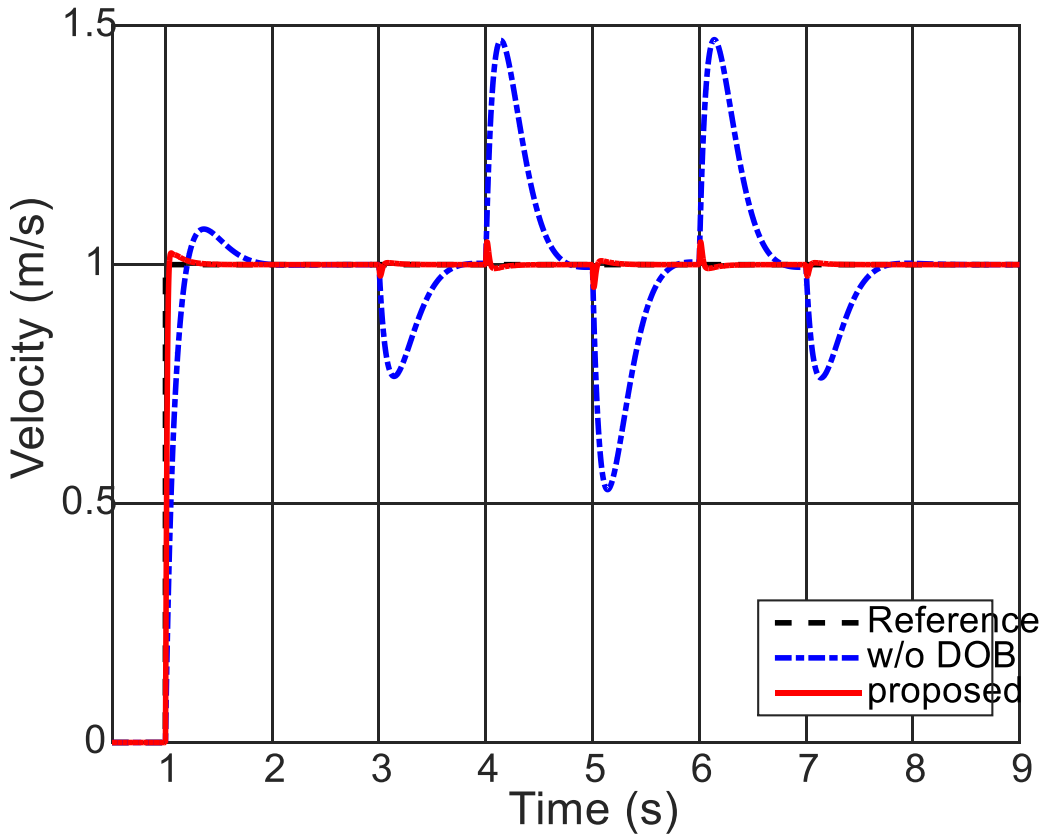


**Figure 4. 8: Square wave**

Figure 4.8 illustrated the three velocity responses of the system under periodic disturbance: (1) the target velocity, (2) the system without a disturbance observer (w/o DOB), and (3) the proposed controller. The black dashed line, representing the reference or target system velocity,

remained constant at 1 m/s throughout the simulation. The blue dashed-dot line, corresponding to the w/o DOB case, exhibited oscillatory behavior caused by the periodic disturbance. The velocity fluctuated significantly, with peak values reaching approximately 1.5 m/s and slopes dropping below 0.8 m/s, which indicated poor disturbance rejection. By contrast, the solid red line representing the proposed controller closely tracked the reference velocity with minimal oscillations, implying that the response remained stable and consistently followed the reference, thereby demonstrating resilience to the applied disturbance.

Compared to Figure 4.7, Figure 4.8 demonstrated that the system without a DOB exhibited poor disturbance rejection, as reflected by the pronounced oscillatory velocity response. This indicated that the periodic disturbances had a direct impact on the system, resulting in significant deviations from the reference velocity. In contrast, the proposed controller provided superior disturbance rejection, maintaining stable operation by effectively attenuating the effects of external perturbations. Its response remained steady and closely tracked the reference throughout the simulation.

The pronounced oscillations in the w/o DOB system revealed its susceptibility to external disturbances, which undermined both the reliability and accuracy of its performance in practical applications. Conversely, the proposed controller enhanced system robustness, making it suitable for operations under dynamic and uncertain conditions, such as in industrial machinery and piston-type (reciprocating) air compressors, where external disturbances were frequently encountered.

**Table 4.5: Comparison of system velocity performance with and without disturbance observer (DOB)**

| System of Measurement | Reference | w/o DOB (Blue) | Proposed (Red) |
|---|---|---|---|
| Peak Velocity (m/s) | 1.0 | 1.48 | 1.05 |
| Min Velocity (m/s) | 1.0 | 0.52 | 0.95 |
| Oscillation Amplitude | 0 | 0.35 | 0.29 |
| Steady-State Error | 0 | 0.02 | 0.01 |

The table presented a comparison of performance metrics between the system operating without a Disturbance Observer (DOB) and the proposed DOB-based configuration. Without DOB, the peak velocity reached 1.48 m/s, exceeding the reference of 1.0 m/s, while the proposed approach maintained it much closer to the target at 1.05 m/s. Regarding minimum velocity, the non-DOB setup declined to 0.52 m/s, far below the reference, whereas the DOB-based system improved the outcome to 0.95 m/s, aligning more closely with the desired value.

With respect to oscillation amplitude, the absence of DOB resulted in larger variations of 0.35, whereas the proposed strategy suppressed them to 0.29, reflecting greater system stability. In addition, steady-state error decreased from 0.02 in the non-DOB case to 0.01 under the DOB context, indicating superior reference tracking.

In summary, the proposed DOB system provided better velocity regulation, attenuated oscillatory behavior, and achieved higher tracking precision compared to the configuration without DOB.

The subsequent step involved evaluating the simulation's accuracy and identifying errors in the estimated disturbances.

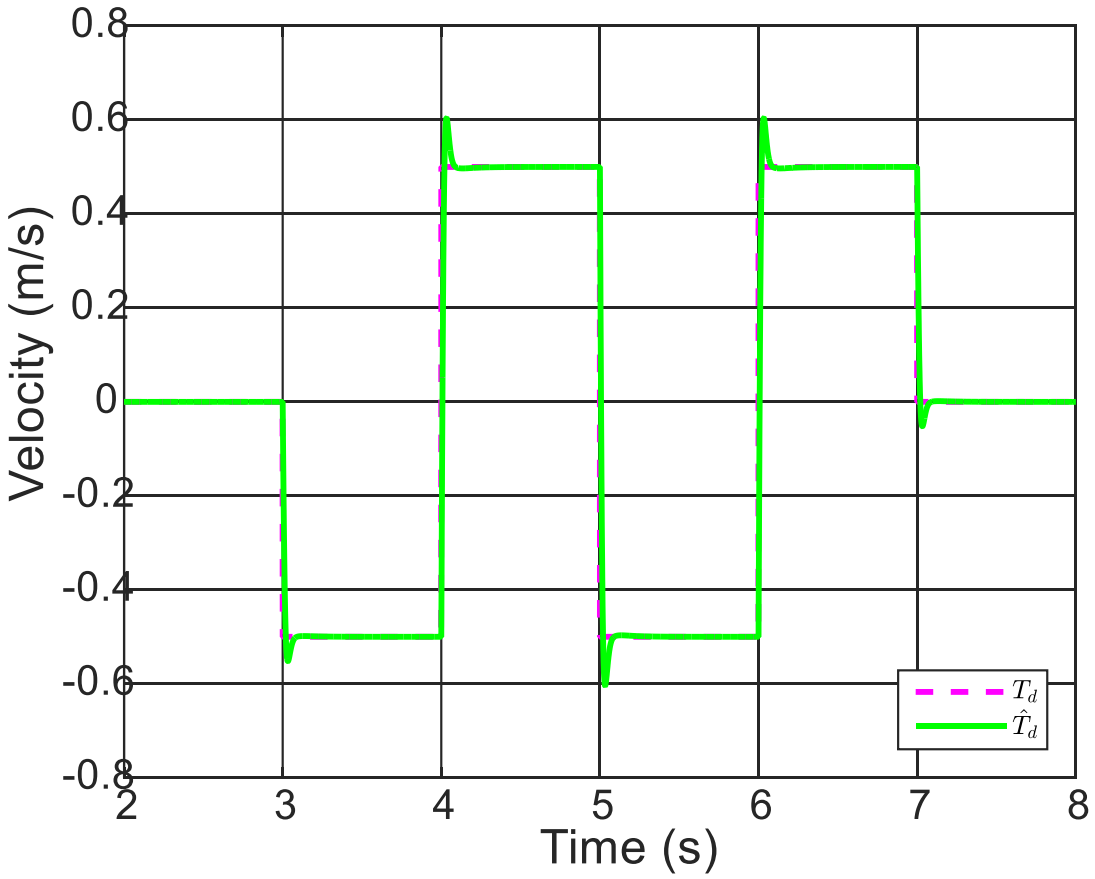


**Figure 4. 9: Comparison of the supplied and estimated disturbance**

Figure 4.9 illustrated the system's disturbance behavior over time. The graph represented a step-like/square waveform with discrete transitions between positive and negative velocities. The two signals $T_d$ and $\hat{T}_d$ were depicted in indicating a comparison of two models. It was recognized that the two signals overlapped closely, suggesting high similarity or negligible error between them.

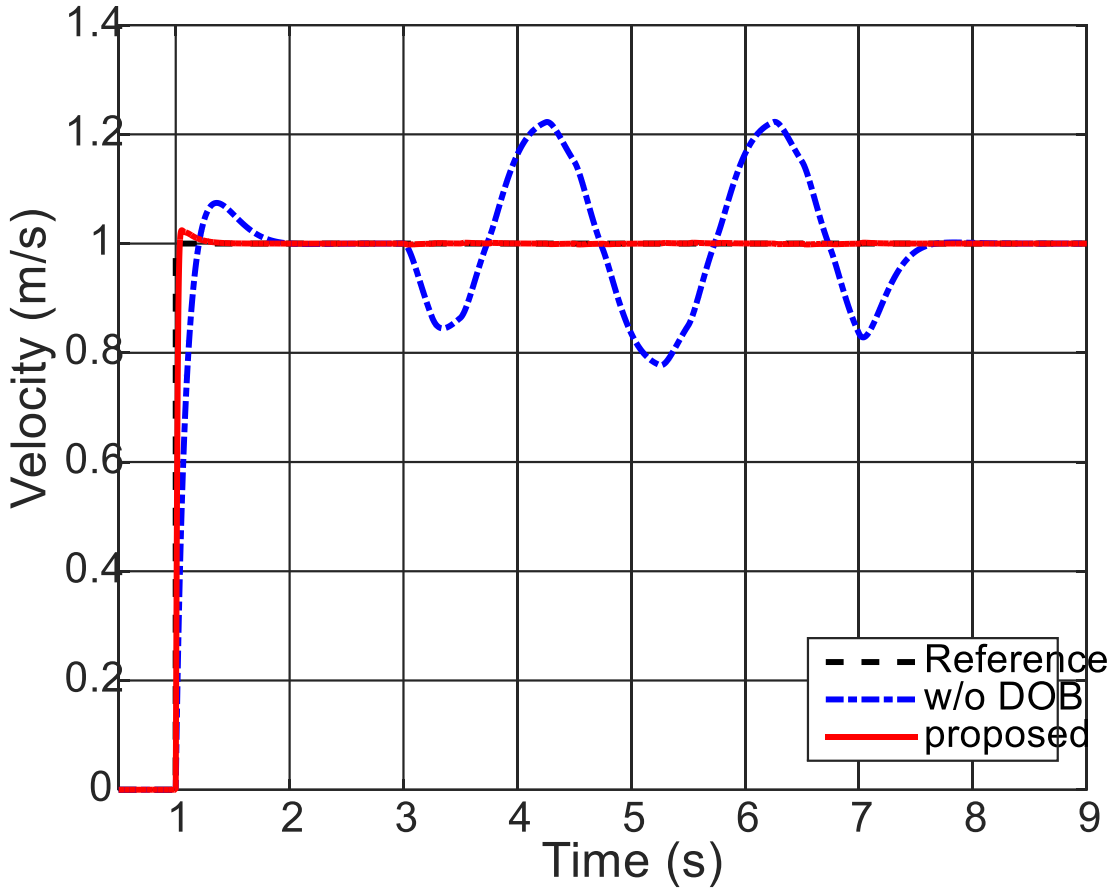


**Figure 4. 10: Sinusoidal Wave**

The graph compared the velocity responses of the system with: (1) the reference velocity (dashed black line), (2) the system without a disturbance observer (w/o DOB, blue dashed line), and (3) the proposed control method (red solid line). The system eventually stabilized over time, but clear differences in tracking accuracy and stability were observed.

The performance of the system without DOB showed significant oscillations with an amplitude of about 0.2 m/s. After the initial rise, it required a longer settling time of 5 seconds, whereas the proposed control method maintained a steady and accurate response throughout the entire time range.

The proposed control method demonstrated superior stability and tracking accuracy compared to the w/o DOB system. The subsequent step involved evaluating the accuracy of the simulation and identifying errors in the estimated disturbances.

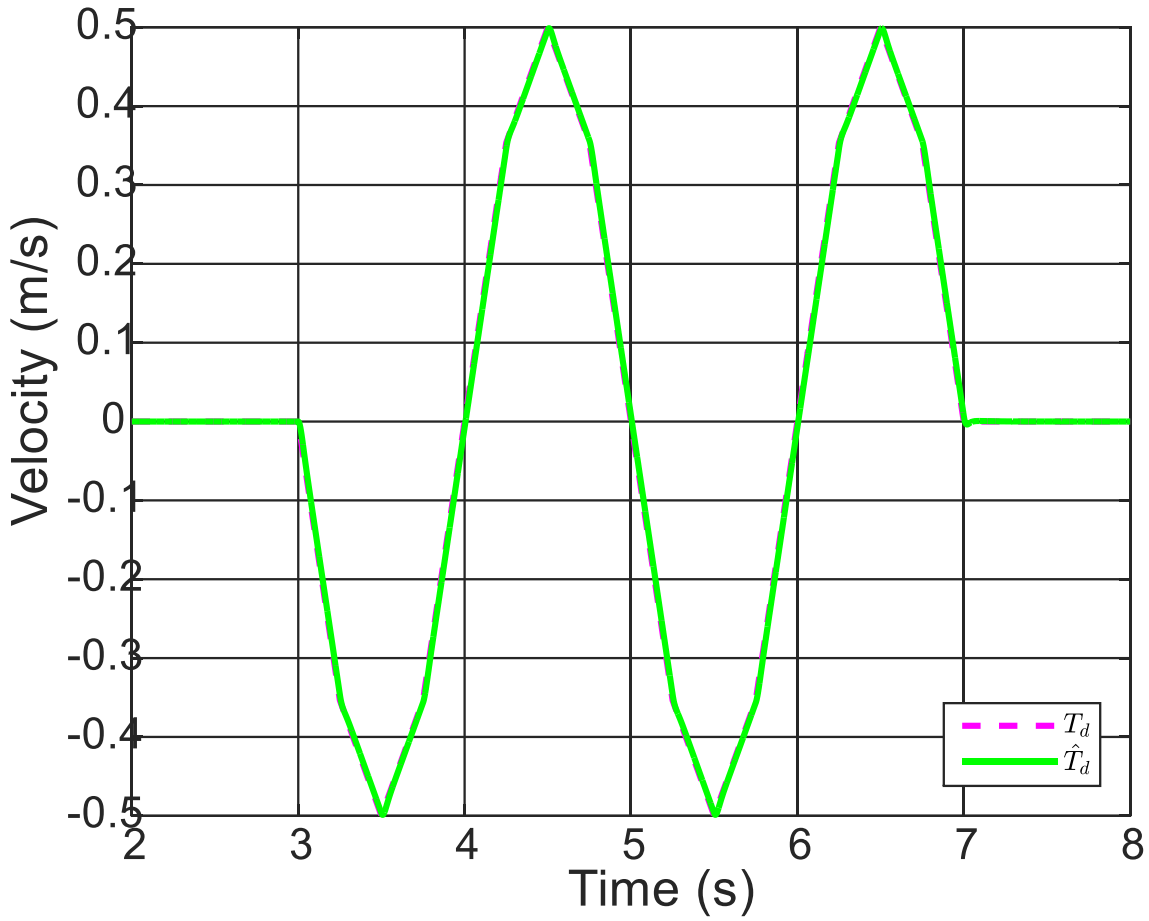


**Figure 4. 11: Comparison between supplied and estimated disturbance**

From the graph, the velocity plot presented a comparison between the supplied disturbance $T_d$ and the estimated disturbance $\hat{T}_d$, illustrating a velocity-time profile for the dynamic system. The system was observed to be accurately estimated, as the estimated disturbance (solid green line) closely tracked the supplied disturbance (purple dashed line). Figure 4.11 showed that the error between the two disturbances was minimal, indicating that the estimation method had a high level of accuracy.

### 4.3.4 Presentation of Results.

The results for the two control configurations were illustrated in Figures 4.5 and 4.6, representing the “no DOB” and the proposed control approach respectively, as displayed in the subsequent figures.

1) Results with Square Disturbances

**Table 4. 6: Square wave**

| System of Measurement | Reference | w/o DOB (Blue) | Proposed (Red) |
|---|---|---|---|
| Peak Velocity (m/s) | 1.0 | 1.5 | 1.0 |
| Min Velocity (m/s) | 1.0 | 0.8 | 1.0 |
| Oscillation Amplitude | 0 | 0.35 | 0 |
| Steady-State Error | 0 | 0 | 0 |

The results from Table 4.5 highlighted the effectiveness of the proposed controller in maintaining stability and rejecting periodic disturbances. Unlike the system without DOB, which exhibited significant oscillations, the proposed controller ensured precise velocity tracking and consistent performance. These findings presented the importance of incorporating robust disturbance compensation strategies to enhance the reliability and stability of dynamic systems.

2) Results with Sinusoidal Disturbances

**Table 4. 7 Results with Sinusoidal disturbances**

| Metrics | Reference (Dashed) | w/o DOB (Blue) | Proposed (Red) |
|---|---|---|---|
| Steady state value | 1.0 | Oscillates around 1.0 | 1.0 |
| Oscillations | None | Significant (amplitude-0.2) | Negligible |
| Settling Time (s) | 1.0 | 5 | 1.0 |
| Tracking Accuracy | Perfect tracking | Deviates due to oscillations | High accuracy |
| Disturbance Rejection | Not applicable | Poor | Excellent |

As presented in Table 4.6, the sinusoidal oscillations observed in the "w/o DOB" case indicated reduced robustness and insufficient stability, which resulted in performance limitations when the system was subjected to disturbances or dynamic variations in operating conditions.

Specifically, the system without DOB oscillated around the steady-state value of 1.0, with a significant oscillation amplitude of approximately 0.2. This instability caused the system to require about 5 seconds to settle, compared to the reference settling time of 1.0 second. Moreover, tracking accuracy was compromised, as the response deviated from the reference due to the oscillatory behaviour, and disturbance rejection was poor.

In contrast, the proposed control method demonstrated superior stability and tracking accuracy by effectively suppressing oscillations. It maintained the steady-state value precisely at 1.0, with negligible oscillations, and achieved a settling time of 1.0 second, thereby matching the reference. Furthermore, the DOB-based approach provided high tracking accuracy and excellent disturbance rejection. Through critical damping, it enhanced both tracking performance and overall system stability, confirming its effectiveness in mitigating oscillatory behaviour and ensuring robust performance.

**Table 4.8: Comparative Analysis of DOB vs Non-DOB Systems**

| Performance Metric | Without DOB | With DOB (Proposed) | Improvement |
|---|---|---|---|
| Rise Time (s) | 0.20 | 0.05 | Faster response (75%) |
| Overshoot (%) | 8% | 2% | Reduced by 75% |
| Settling Time (s) | 0.70 | 0.15 | Reduced by 78.5% |
| Steady-State Error | 0.02 | 0.01 | 50% reduction |

It was observed in Table 4.8 that a direct comparison was made between the performance of the system using a conventional feedback controller (without DOB) and the proposed Disturbance Observer-Based (DOB) control system. The comparison was based on key performance indicators such as rise time, overshoot, settling time, and steady-state error metrics used to evaluate the speed, stability, and accuracy of the control system.

According to the findings, the rise time improved significantly with the DOB controller, decreasing from 0.20 seconds to 0.05 seconds. This was interpreted to mean that the system responded much more rapidly to input changes, which was particularly valuable for applications demanding quick and precise control, such as industrial compressors.

The study further reported that overshoot was reduced from 8% to 2%, indicating that the DOB controller was effective in damping system responses and minimizing excessive deviation from the target value. This reduction was considered important for vibration-prone systems like piston-type compressors, where high overshoot could lead to mechanical stress and operational instability.

Additionally, it was noted that the settling time improved from 0.70 seconds to 0.15 seconds, showing that the system returned to steady operation more quickly following a disturbance. This improvement demonstrated the DOB controller's effectiveness in maintaining system stability.

The steady-state error also decreased slightly from 0.02 to 0.01, which, although a minor improvement, reflected enhanced tracking accuracy.

3) Estimation of Disturbances

**Table 4.8: Results from comparison between supplied and estimated disturbance (Square wave)**

| **Time (s)** | $T_d$**(m/s)** | $\widehat{T}_d$**(m/s)** | **Remarks** |
|---|---|---|---|
| **3.0** | -0.5 | -0.55 and stabilizes at -0.5 | Initial steady state |
| **4.0** | 0.5 | Peak at 0.6 and stabilizes at 0.5 | First step change |
| **5.0** | -0.5 | -0.6 | Second step change |
| **6.0** | 0.5 | 0.6 | Third step change |
| **7.0** | 0.0 | -0.05 | Fourth step change |

From the tabulated results in Table 4.8, the graph demonstrated a clear periodic behavior in velocity, alternating between positive and negative values at consistent intervals of (-0.6 m/s to 0.6m/s). This behavior suggested a system operating in a periodic or oscillatory manner.

**Table 4.9: Comparison between supplied and estimated disturbance (Sinusoidal wave)**

| **Metric** | $T_1$ **(Dashed Magenta line)** | $T_2$ **(Solid green line)** |
|---|---|---|
| Peak Velocity (m/s) | 0.5 | 0.5 |
| Minimum Velocity (m/s) | -0.5 | -0.5 |
| Periodicity (s) | 2.0 | 2.0 |
| Steady-state value (m/s) | 0.0 | 0.0 |
| Phase difference | Nearly identical | Nearly identical |
| Overall Behavior | Matches $T_2$ closely | Matches $T_1$closely |

The two curves ($T_1$ d $T_2$) were almost identical in magnitude, behavior, suggesting consistent performance or synchronization between the two variables over the observed time interval.

# CHAPTER FIVE: SUMMARY, CONCLUSIONS AND RECOMMENDATIONS

## 5.0 Summary

The research presented a comprehensive evaluation of the effectiveness of the developed model in suppressing vibrations in piston-type air compressors. It was reported that a high-fidelity dynamic simulation model had been established, accurately capturing the motor and mechanical characteristics of the compressor system. The study indicated that the integration of a Disturbance Observer-Based (DOB) control strategy significantly enhanced the system's ability to attenuate vibrations.

Model validation, carried out by comparing supplied and estimated disturbances, was said to confirm the model's accuracy in replicating the compressor's dynamic response under varying operational conditions. The researchers reported that the DOB-based control system outperformed conventional methods by improving essential performance metrics such as rise time, overshoot, and settling time factors considered critical for stable and efficient operation. Furthermore, it was noted that the tuning of control parameters, including motor torque regulation and disturbance rejection, demonstrated the model's effectiveness in real-time control, contributing to greater operational efficiency and reduced mechanical wear.

## 5.1 Conclusion

The study concludes that the proposed robust control system, based on the Disturbance Observer (DOB), is an effective solution for mitigating excessive vibrations in piston-type air compressors. Simulation results show that the DOB control strategy provides superior vibration suppression compared to traditional feedback control techniques. The model successfully captured the dynamic behaviour of the compressor system and adapted to varying operating conditions, ensuring long-term reliability and optimal performance.

### 5.1.1 Key findings from the study

- It was found that a comprehensive simulation model was successfully developed, capable of accurately capturing the real-time dynamic behaviour of the compressor system under varying operating conditions.
- The study reported that the implementation of a Disturbance Observer-Based (DOB) control strategy resulted in a significant improvement in vibration suppression compared to traditional control methods.
- Specifically, the estimated equivalent moment of inertia decreased from 0.1063 to 0.04252 with DOB, indicating a more responsive system. Additionally, the PID controller gains increased substantially $K_p$ rose from 1.2039 to 3.3176, $K_I$ from 6.2595 to 28.3885, and $K_D$ from 0.0167 to 0.02096, allowing for faster response and better disturbance rejection.
- It was observed that the system's dynamic performance improved considerably, with notable reductions in rise time, overshoot, and settling time parameters essential for assessing the stability and responsiveness of the control system.
- The control parameters were reported to have been effectively tuned, particularly in the areas of motor torque regulation and disturbance rejection, leading to enhanced system adaptability and real-time control capability.
- The accuracy of the developed model was validated, as simulation results closely matched actual system responses, demonstrating its reliability for predictive and control purposes.
- The study further indicated that the optimized control strategy led to greater operational efficiency and reduced mechanical wear by minimizing vibration-induced stresses and dynamic fluctuations within the compressor system.

## 5.2 Recommendations

Based on the research findings and analysis, the following recommendations were proposed to further enhance the practicality and performance of the developed DOB control system:

- **Implementation of DOB Control Systems**: It is recommended that industrial applications using piston-type air compressors adopt the DOB-based control system to improve vibration suppression, reduce energy consumption, minimize mechanical stress, and lower maintenance costs.
- **Further Optimization of Control Parameters**: Future research should focus on further refining the control parameters to optimize performance across a wider range of operating conditions. This could involve incorporating machine learning techniques to allow for adaptive control adjustments in real time.
- **Real-World Testing**: Although the model demonstrated strong performance in simulations, it is advisable to conduct real-world testing on actual compressor systems to validate the practical applicability and effectiveness of the DOB control strategy.
- **Integration with Predictive Maintenance**: The developed model and control system could be integrated with predictive maintenance systems to monitor the health of compressors in real-time, enabling early detection of potential failures and enhancing system reliability and longevity.
- **Expansion to other compressor types**: The methodology developed in this study can be adapted to other types of compressors, both reciprocating and rotary, with minimal adjustments to the model and control approach, potentially offering widespread benefits across various industrial applications.

## REFERENCES


Aboelhassan, A., Abdelgeliel, M., Zakzouk, E. E., & Galea, M. (2020). Design and Implementation of Model Predictive Control-Based PID Controller for Industrial Applications. *Energies*, *13*(24).

Almasi, A. (2016). Latest Practical Notes and Recent Lessons Learned on Reciprocating Compressors. *Australian Journal of Mechanical Engineering*, *14*(2), 138–150.

Amiebenomo, S. O., Udeji, F. O., & Aigbokie, J. I. (2023). *Design and Fabrication of a 4 Bar Air Compressor*.

Aw, K. T., & Ooi, K. T. (2021). A review on sliding vane and rolling piston compressors. *Machines*, *9*(6). https://doi.org/10.3390/machines9060125

Ben Mansour, R., Ouzzane, M., & Aidoun, Z. (2014). Numerical evaluation of ejector-assisted mechanical compression systems for refrigeration applications. *International Journal of Refrigeration*, *43*, 36–49. https://doi.org/10.1016/j.ijrefrig.2014.04.010

Bonfá, F., Benedetti, M., Ubertini, S., Introna, V., & Santolamazza, A. (2019). New Efficiency Opportunities Arising from Intelligent Real Time Control Tools Applications: The Case of Compressed Air Systems' Energy Efficiency In Production and Use. *Energy Procedia*, *158*, 4198–4203. https://doi.org/10.1016/j.egypro.2019.01.809

Carletti, E., & Pedrielli, F. (2019). Noise and Vibration Risk Assessment for the Operators of Crawler Loaders. *Archives of Acoustics*, *44*(4), 761–773. https://doi.org/10.24425/aoa.2019.129731

Caruana, L., & Refalo, P. (2018). Sustainability Analysis of a Compressed Air System. *Engineering Sustainability & Sustainable Energy (Esse)*, *May 2018*, 38–45. https://www.researchgate.net/publication/335293928

Chai, K., Lou, J., & Yang, Y. (2023). Mechanical Performance Analysis and Experimental Study of Four-Star-Type Crank-Linkage Mechanism. *Applied Sciences (Switzerland)*, *13*(14). https://doi.org/10.3390/app13148202

Chen, W. H., Yang, J., Guo, L., & Li, S. (2016). Disturbance-Observer-Based Control and Related Methods - An Overview. *IEEE Transactions on Industrial Electronics*, *63*(2), 1083–1095. https://doi.org/10.1109/TIE.2015.2478397

Cheng, S., & Liu, S. (2017). Dynamics Analysis of Reciprocating Compressor with a Clearance between Crankshaft and Connecting Rod. *Vibroengineering Procedia*, *15*, 38–43. https://doi.org/10.21595/vp.2017.19285

Chu, T., Nguyen, T., Yoo, H., & Wang, J. (2024). A review of vibration analysis and its applications. *Heliyon*, *10*(5), e26282. https://doi.org/10.1016/j.heliyon.2024.e26282

Das, O., Bagci Das, D., & Birant, D. (2023). Machine learning for fault analysis in rotating machinery: A comprehensive review. *Heliyon*, *9*(6), e17584. https://doi.org/10.1016/j.heliyon.2023.e17584

Egorov, A. V., Lysyannikov, A. V., Kaizer, Y. F., Andryuhin, N. S., Dorohin, S. V., Kuznetsov, A. V., Bogdanov, E. N., & Lysyannikova, N. N. (2019). Dynamic Method of Controlling Friction Losses in the Mechanism of Converting Reciprocating Motion into Rotary Inline Piston Internal Combustion Engines. *Journal of Physics: Conference Series*, *1399*(4). https://doi.org/10.1088/1742-6596/1399/4/044078

Eklind, V., & Karlsson, J. (2019). *Development of a Predictive Maintenance Algorithm for Detection of Faulty Drive Belts*.

Ghazwani, M. H., & Pham, V. V. (2024). Investigating Behavior of Slider–Crank Mechanisms with Bearing Failures Using Vibration Analysis Techniques. *Mathematics*, *12*(4).

https://doi.org/10.3390/math12040544

Gupta, R., Moazamigoodarzi, H., MirhoseiniNejad, S. M., Down, D. G., & Puri, I. K. (2020). Workload management for air-cooled data centers: An energy and exergy based approach. *Energy*, *209*, 118485. https://doi.org/10.1016/j.energy.2020.118485

Halicioglu, R., Dulger, L. C., & Bozdana, A. T. (2014). Modelling and simulation based on matlab/simulink: A press mechanism. *Journal of Physics: Conference Series*, *490*(1), 1–6. https://doi.org/10.1088/1742-6596/490/1/012053

Hoag, K., & Dondlinger, B. (2015). Vehicular engine design: Second edition. *Vehicular Engine Design: Second Edition*, 1–386. https://doi.org/10.1007/978-3-7091-1859-7

Hong, D., Qiu, Y., & Kim, B. (2023). Vibration Characteristics of an Active Mounting System for Motion Control of a Plate-like Structure in Future Mobilities. *Scientific Reports*, *13*(1), 1–17. https://doi.org/10.1038/s41598-023-43419-w

Hu, K., Zhang, G., & Zhang, W. (2022). Analysis and Design of Electromagnetic Vibration and Noise Reduction Method of Permanent Magnet Motor. *Journal of Low Frequency Noise Vibration and Active Control*, *41*(1), 359–373. https://doi.org/10.1177/14613484211038405

Jani, D. B., Raj, C., Amit, B., Sandip, B., Jignesh, B., & Murtza, B. (2019). *Performance Investigation on Double Stage Reciprocating Air Compressor*. *6*(4), 142–146.

Jiang, G., Wang, Y., Li, F., & Jing, X. (2021). An Integrated Nonlinear Passive Vibration Control System and its Vibration Reduction Properties. *Journal of Sound and Vibration*, *509*, 116231. https://doi.org/10.1016/j.jsv.2021.116231

Kacani, V. (2017). Vibration analysis in reciprocating compressors. *IOP Conference Series:*

*Materials Science and Engineering*, *232*(1). https://doi.org/10.1088/1757-899X/232/1/012016

Kang, T. J., Yang, C., Park, Y., Hyun, D., Lee, S. Bin, & Teska, M. (2018). Electrical Monitoring of Mechanical Defects in Induction Motor-Driven V-Belt-Pulley Speed Reduction Couplings. *IEEE Transactions on Industry Applications*, *54*(3), 2255–2264. https://doi.org/10.1109/TIA.2018.2805840

Kavya, M., & Jayalalitha, S. (2022). A novel coarse and fine control algorithm to improve Maximum Power Point Tracking (MPPT) efficiency in photovoltaic system. *ISA Transactions*, *121*(xxxx), 180–190. https://doi.org/10.1016/j.isatra.2021.03.036

Khan, D., & Burdzik, R. (2023). Measurement and Analysis of Transport Noise and Vibration: A review of Techniques, Case Studies, and Future directions. *Measurement: Journal of the International Measurement Confederation*, *220*(June). https://doi.org/10.1016/j.measurement.2023.113354

Kostyukov, V. N., & Naumenko, A. P. (2016). About the Experience in Operation of Reciprocating Compressors under Control of the Vibration Monitoring System. *Procedia Engineering*, *152*, 497–504. https://doi.org/10.1016/j.proeng.2016.07.635

Kotlov, A. A. (2019). Research of Two-stage Reciprocating Compressor by Methods of Physical and Mathematical Experiments. *AIP Conference Proceedings*, *2141*(August). https://doi.org/10.1063/1.5122071

Krot, P., Korennoi, V., & Zimroz, R. (2020). Vibration-based Diagnostics of Radial Clearances and Bolts Loosening in the Bearing Supports of the Heavy-duty Gearboxes. *Sensors (Switzerland)*, *20*(24), 1–20. https://doi.org/10.3390/s20247284

Li, Y., Li, Y., Ji, P., & Yang, J. (2015). Development of energy storage industry in China: A

technical and economic point of review. *Renewable and Sustainable Energy Reviews*, *49*, 805–812. https://doi.org/10.1016/j.rser.2015.04.160

Liang, Z., Li, S., Tian, J., Zhang, L., Feng, C., & Zhang, L. (2015). Vibration cause analysis and elimination of reciprocating compressor inlet pipelines. *Engineering Failure Analysis*, *48*, 272–282. https://doi.org/10.1016/j.engfailanal.2014.11.003

Lipus, J., Jankovych, R., Hammer, M., & Lipus, T. (2016). Vibration and Related Diagnostics of Motors and Generators. *MM Science Journal*, *2016*(DECEMBER), 1639–1642. https://doi.org/10.17973/MMSJ.2016_12_2016202

Lu, K., Sultan, I. A., & Phung, T. H. (2023). A Literature Review of the Positive Displacement Compressor: Current Challenges and Future Opportunities. *Energies*, *16*(20). https://doi.org/10.3390/en16207035

Lu, Z. Q., Gu, D. H., Ding, H., Lacarbonara, W., & Chen, L. Q. (2020). Nonlinear Vibration Isolation via a Circular Ring. *Mechanical Systems and Signal Processing*, *136*. https://doi.org/10.1016/j.ymssp.2019.106490

Maduna, L., & Patnaik, A. (2017). Textiles in air filtration. *Textile Progress*, *49*(4), 173–247. https://doi.org/10.1080/00405167.2018.1461921

Mantri, P., & Tamma, B. (2014). *Friction Model Development for a reciprocating compressor*.

Marvania, D., & Subudhi, S. (2017). A comprehensive review on compressed air powered engine. *Renewable and Sustainable Energy Reviews*, *70*(August 2015), 1119–1130. https://doi.org/10.1016/j.rser.2016.12.016

Meroni, A., Zühlsdorf, B., Elmegaard, B., & Haglind, F. (2018). Design of Centrifugal Compressors for Heat Pump Systems. *Applied Energy*, *232*(September), 139–156.

https://doi.org/10.1016/j.apenergy.2018.09.210

Mi, J., & Meng, Y. (2014). Numerical Analyses of Hydrodynamic Lubrication and Dynamics of the Rolling Piston and Crankshaft in a Rotary Compressor. *Tribology Transactions*, *57*(6), 1136–1147. https://doi.org/10.1080/10402004.2014.941082

Mohamed Hussein M. Faris, Elamin Elhussein, Hassan Osman Ali, & Ali Yousif. (2019). A Review of Applied Modern Condition Monitoring and Best Maintenance Engineering Practices in Reciprocating Gas Compression Plants. *International Journal of Engineering Research and Technology*, *12*(12), 2983–2987.

Mohd Ghazali, M. H., & Rahiman, W. (2021). Vibration Analysis for Machine Monitoring and Diagnosis: A Systematic Review. *Shock and Vibration*, *2021*. https://doi.org/10.1155/2021/9469318

Mu-jun, X. I. E., & Jian, L. I. U. (2010). Design and Simulation of air Compressor Performance Controller. *Design and Simulation of Air Compressor Performance Controller*, 504–506.

Muzakkir, S. M., & Kumar, S. (2015). Design of mechanical oil seal and gasket. *International Journal of Applied Engineering Research*, *10*(12), 30911–30926.

MWE. (2013). Water Supply Design Manual-Second Edition. The Republic of Uganda, Ministry of Water and Environment. *Government of Uganda*, *3*, 3–26.

Nair, V. G., Hegde, N. T., & Dileep, M. V. (2024). *Active Vibration Isolation using Tilt Horizontal Coupling Immune Inertial Double Link Sensor for Low Frequency Applications*. *5*(6), 1673–1689. https://doi.org/10.18196/jrc.v5i6.22595

Namata Edith. (2023). *Analysis of the Role of Renewable Energy Towards Successful Implementation of Sustainable Development Pillars" A Case Study of Uganda*. *May*, 1–

14. https://www.ncbi.nlm.nih.gov/books/NBK558907/

Nehler, T., Parra, R., & Thollander, P. (2018). Implementation of Energy Efficiency Measures in Compressed Air Systems: Barriers, Drivers and Non-Energy Benefits. *Energy Efficiency*, *11*(5), 1281–1302. https://doi.org/10.1007/s12053-018-9647-3

Nigus, H. (2018). *Kinematics and Load Formulation of Engine Crank Hailemariam Nigus to Cite this Version : HAL Id : hal-01305936*. *March*.

Nourin, F. N., Espindola, J., Selim, O. M., & Amano, R. S. (2022). Energy, Exergy, and Emission Analysis on Industrial Air Compressors. *Journal of Energy Resources Technology, Transactions of the ASME*, *144*(4), 1–14. https://doi.org/10.1115/1.4051682

Olabi, A. G., Wilberforce, T., Ramadan, M., Abdelkareem, M. A., & Alami, A. H. (2021). Compressed Air Energy Storage Systems: Components and Operating Parameters – A Review. *Journal of Energy Storage*, *34*(August), 102000. https://doi.org/10.1016/j.est.2020.102000

Park, J. K., Kim, D., Kim, Y., & Kim, S. K. (2024). Order Reduction Adaptive Current Tracking Control with Proportional–Integral-Type Filter for MAGLEV Applications. *Machines*, *12*(12), 1–16. https://doi.org/10.3390/machines12120880

Peyvan, A., & Benisi, A. H. (2016). Axial-flow Compressor Performance Prediction in Design and Off-design Conditions through 1-D and 3-D Modeling and Experimental Study. *Journal of Applied Fluid Mechanics*, *9*(5), 2149–2160. https://doi.org/10.18869/acadpub.jafm.68.236.25222

Pipalia, V. F., Shukla, D. D., & Mehta, N. C. (2016). *Investigation on Reciprocating Air Compressors -a Review*. *December*.

Porwal, C. G. (2015). *High Specific Speed in Circulating Water Pump Can Cause Cavitation , Noise and Vibration*. *201301*(12), 2053–2065.

Ramezani-al, M. R., Tavanaei-Sereshki, Z., & Emami, K. (2023). A finite-time Adaptive Sliding Mode Control Based on DOB for AUVs subject to Matched and Mismatched Disturbances. *Transactions of the Institute of Measurement and Control*, *45*(10), 1873–1885. https://doi.org/10.1177/01423312221138988

Robison, D. H., & Beaty, P. J. (2013). Compressor Types, Classifications, and Applications. *The Twenty-First Turbomachinery Symposium*, *1*, 183–188.

Salem, F. M., Mosaad, M. I., & Awadallah, M. A. (2015). A comparative study of MPC and optimised PID control. *International Journal of Industrial Electronics and Drives*, *2*(4), 242. https://doi.org/10.1504/ijied.2015.076293

Samuel, B. E., & Parthiban, L. (2016). *Time Systems*. *2*(1), 123–126.

Samuel, K. (2023). *Development of Advanced Robot Force Control Algorithms*.

Samuel, K., Haninger, K., Oboe, R., Haddadin, S., & Oh, S. (2024). A Perturbation-Robust Framework for Admittance Control of Robotic Systems with High-Stiffness Contacts and Heavy Payload. *IEEE Robotics and Automation Letters*, *9*(7), 6432–6439. https://doi.org/10.1109/LRA.2024.3406055

Samuel, K., Haninger, K., Oboe, R., & Oh, S. (2024). Outer-Loop Admittance and Motion Control Dual Improvement via a Multi-Function Observer. *IEEE Transactions on Industrial Electronics*, *71*(8), 9339–9350. https://doi.org/10.1109/TIE.2023.3317843

Samuel, K., Kim, J., & Oh, S. (2021). Performance Comparison of Position Controlled Robotic Stage When Force-and Position-Based Disturbance Observers are Implemented.

*International Conference on Control, Automation and Systems*, *2021-Octob*(Iccas), 994–999. https://doi.org/10.23919/ICCAS52745.2021.9649946

Samuel, K., & Oh, S. (2022). A Comparative Study of Force Observers For Accurate Force Control of Multisensor-Based Force Controlled Motion Systems. *IEEE International Conference on Intelligent Robots and Systems*, *2022-Octob*, 11223–11230. https://doi.org/10.1109/IROS47612.2022.9981321

Shu, M., Yang, M., Zhang, K., Deng, K., Yang, B., & Martinez-Botas, R. (2019). Experimental Study on Performance of Centrifugal Compressor Exposed to Pulsating Backpressure. *Aerospace Science and Technology*, *95*, 105450. https://doi.org/10.1016/j.ast.2019.105450

Söderfjäll, M. (2017). *Friction in Piston Ring - Cylinder Liner Contacts*. http://www.diva-portal.org/smash/get/diva2:1076831/FULLTEXT01.pdf

Sriraman, A. (2023). *Design of Belt Drive Mechanism for Better Efficiency and Life*. *January*.

Tempiam, A., Kachapongkun, P., Rattanadecho, P., & Prommas, R. (2020). Experimental investigation of vortex tube for reduction air inlet of a reciprocating air compressor. *Case Studies in Thermal Engineering*, *19*(February), 100617. https://doi.org/10.1016/j.csite.2020.100617

Tiainen, J., Grönman, A., Jaatinen-Värri, A., & Backman, J. (2018). Flow Control Methods and their Applicability in Low-Reynolds-Number Centrifugal Compressors - A review. In *International Journal of Turbomachinery, Propulsion and Power* (Vol. 3, Issue 1). https://doi.org/10.3390/ijtpp3010002

Townsend, J., Badar, M. A., & Szekerces, J. (2016). Updating Temperature Monitoring on Reciprocating Compressor Connecting Rods to Improve Reliability. *Engineering Science*

*and Technology, an International Journal*, *19*(1), 566–573. https://doi.org/10.1016/j.jestch.2015.09.012

Tran, V. T., Althobiani, F., & Ball, A. (2014). An Approach to Fault Diagnosis of Reciprocating Compressor Valves Using Teager-Kaiser Energy Operator and Deep Belief Networks. *Expert Systems with Applications*, *41*(9), 4113–4122. https://doi.org/10.1016/j.eswa.2013.12.026

Urakawa, Y. (2019). Vibration Suppression in /Position Control System by Pole Zero Cancellation using Limited Pole Placement Method. *IEEJ Journal of Industry Applications*, *8*(2), 256–262. https://doi.org/10.1541/ieejjia.8.256

Veysi, P., Adeli, M., & Naziri, N. P. (2024). *Introduction to PID Controller and Model Predictive Control in Engineering Introduction to PID Controller and Model Predictive Control in Engineering Systems*. *April*.

Wang, Y., & Yan, J. (2024). Study of Performance Changes in Centrifugal Compressors Working in Different Refrigerants. *Energies* , *17*(11). https://doi.org/10.3390/en17112784

Wasbari, F., Bakar, R. A., Gan, L. M., Tahir, M. M., & Yusof, A. A. (2017). A review of compressed-air hybrid technology in vehicle system. *Renewable and Sustainable Energy Reviews*, *67*, 935–953. https://doi.org/10.1016/j.rser.2016.09.039

Yin, F., Gao, Q., & Sun, J. (2024). Research and Application of the Simulation Method for Product Development Process Based on System Dynamics. *Systems*, *12*(5). https://doi.org/10.3390/systems12050172

Yin, H., Ramli, R., Saifizul, A., & Foong, M. (2020). Detection and Estimation of Valve Leakage Losses in Reciprocating Compressor Using Acoustic Emission Technique. *Measurement*, *152*, 107315. https://doi.org/10.1016/j.measurement.2019.107315

Zhang, H., Wu, J., Xie, F., Chen, A., & Li, Y. (2014). Dynamic Behaviors of the Crankshafts in Single-cylinder and Twin-cylinder Rotary Compressors. *International Journal of Refrigeration*, *47*, 36–45. https://doi.org/10.1016/j.ijrefrig.2014.07.014

Zhang, X., Ziviani, D., Braun, J. E., & Groll, E. A. (2018). *Modeling the Dynamic Characteristics and Performance of Linear Compressors*. *July*, 1–11.

Zhang, X., Ziviani, D., Groll, E., Braun, J. E., & Groll, E. A. (2017). *A Numerical Study on Dynamic Characteristics of Linear Compressor for Electronics Cooling Chemical Looping Heat Pumps View project Vapor Compression Cooling for Spacecraft View project A Numerical Study on Dynamic Characteristics of Linear Compressor for . March 2018*. https://www.researchgate.net/publication/319016077

Zhao, F., Li, H., Li, H., & Liu, D. (2023). Experimental Investigation of Vibration Reduction Effect of High-Pressure Air Compressor Using Composite Damping Base. *Machines*, *11*(2), 1–13. https://doi.org/10.3390/machines11020229

Zhao, Y., Feng, J., Zhao, B., Zhou, S., Tang, Z., & Peng, X. (2019). Vibration analysis and control of a screw compressor outlet piping system. *Proceedings of the Institution of Mechanical Engineers, Part E: Journal of Process Mechanical Engineering*, *233*(2), 403–411. https://doi.org/10.1177/0954408918763561

Žiaran, S., Šooš, L., & Chlebo, O. (2020). The Primary Noise Control in the Work Environment by Increasing the Quality of Bearings and Effective Mounting of Machines. *Archives of Acoustics*, *45*(2), 253–262. https://doi.org/10.24425/aoa.2020.133146

## APPENDIX A

```
% Matlab code:

% Parameters

K_G = 2; % Steady-state value (final value)

tau = 0.1; % Time constant

% Time vector

t = 0:0.02:1.2; % Time from 0 to 1.2 seconds with small increments


% Step response equation

y = K_G * (1 - exp(-t / tau));


% Plot the response

figure;

plot(t, y, 'b', 'LineWidth', 2); % Plot the response in blue with line width 2

hold on;

y_line(K_G, '--r', 'Final Value (K_G)'); % Plot the final value K as a reference

x_line(tau, '--g', 't = \tau'); % Plot the time constant tau for reference


% Labels and title

xlabel('Time (seconds)');

ylabel 'Response y(t)');

title('Step Response: y(t) = K_G(1 - e^{(-t/\tau)})');

ylim([0 2)

grid on;
```

# APPENDIX B

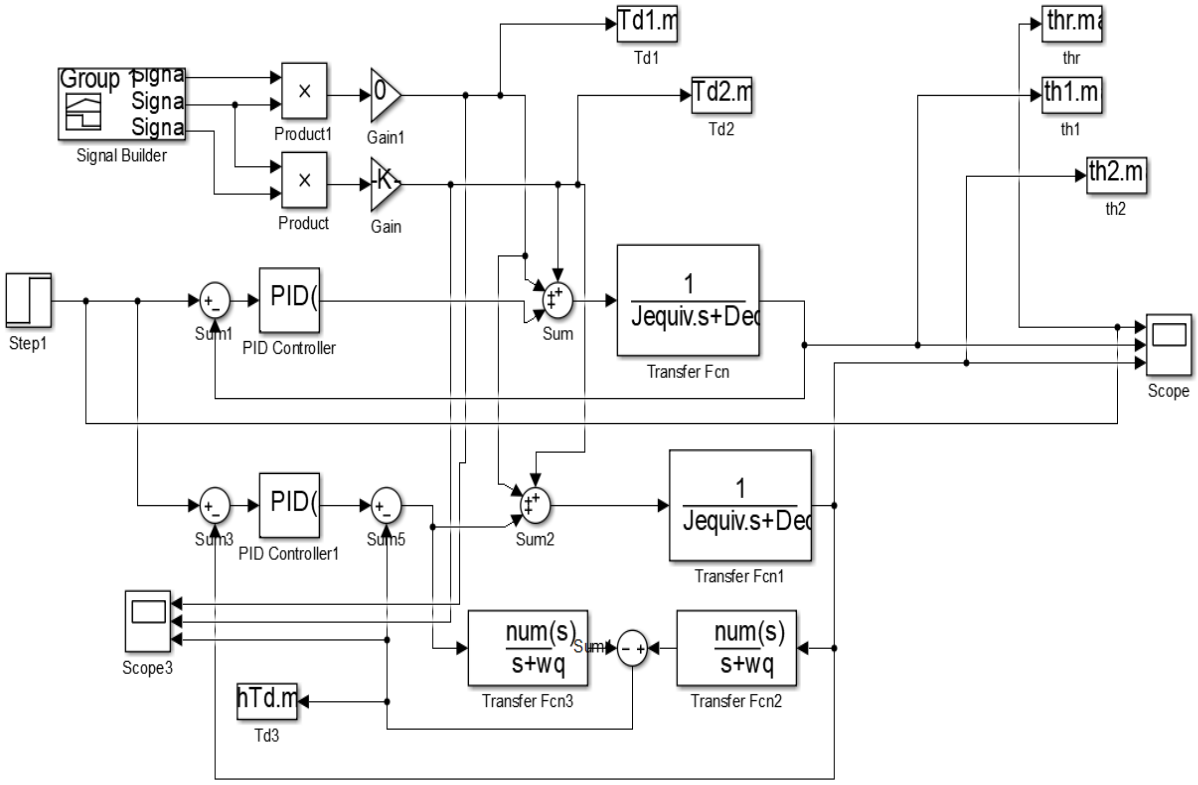


*The Simulink Block Diagram*

## APPENDIX C

Matlab Code for the Simulink Block Diagram.

```
clear all;

close all;


% Jequiv = 2.96e-7 + 0.1* 1.031*1.031;

% Dequiv = 1.323e-5 + 0.2222 * 1.031*1.031;

% hJequiv = Jequiv*0.4;

% hDequiv = Dequiv*1;

% wq = 2*pi*30;


%% plots

% load('hTd.mat'); hTdp = hTd(2,:);

% load('Td1.mat'); Td1p = Td1(2,:);

% load('Td2.mat'); Td2p = Td2(2,:);

% load('thr.mat'); thrp = thr(2,:);

% load('th1.mat'); th1p = th1(2,:);

% load('th2.mat'); th2p = th2(2,:);


%% no disturbance

t = 0:1/1000:10;


load('no dist.mat');

figure;

plot(t,thrp,'--k','LineWidth',2); hold on
```

```
plot(t,th1p,'-.b','LineWidth',2); hold on
plot(t,th2p,'-r','LineWidth',2); hold off
grid on
legend('Reference','w/o DOB','proposed','location','southeast');
xlabel('Time (s)'); ylabel('Velocity (m/s)');
xlim([0.5 2.5]);

%% disturbance 1
load('dist 1.mat');
figure;
plot(t,thrp,'--k','LineWidth',2); hold on
plot(t,th1p,'-.b','LineWidth',2); hold on
plot (t, th2p,'-r','LineWidth',2); hold off
grid on
legend ('Reference','w/o DOB ',' proposed ',' location ',' southeast');
xlabel ('Time (s)'); ylabel ('Velocity (m/s)');
xlim ([0.5 9]);

figure;
plot(t,Td1p,'--m','LineWidth',2); hold on
plot(t,hTdp,'-g','LineWidth',2); hold off
grid on

legend('$T_d$','$\hat{T}_d$','interpreter','latex','location','southeast');
xlabel('Time (s)'); ylabel('Velocity (m/s)');
xlim([2 8]);
```

```
%% disturbance 2
load('dist 2.mat');
figure;
plot(t,thrp,'--k','LineWidth',2); hold on
plot(t,th1p,'-.b','LineWidth',2); hold on
plot(t,th2p,'-r','LineWidth',2); hold off
grid on

legend('Reference','w/o DOB','proposed','location','southeast');
xlabel('Time (s)'); ylabel('Velocity (m/s)');
xlim([0.5 9]);

figure;
plot(t,Td2p,'--m','LineWidth',2); hold on
plot(t,hTdp,'-g','LineWidth',2); hold off
grid on

legend('$T_d$','$\hat{T}_d$','interpreter','latex','location','southeast');
xlabel('Time (s)'); ylabel('Velocity (m/s)');
xlim([2 8]);

clear all;
close all;

% Jequiv = 2.96e-7 + 0.1* 1.031*1.031;
```

```
% Dequiv = 1.323e-5 + 0.2222 * 1.031*1.031;
% hJequiv = Jequiv*0.4;
% hDequiv = Dequiv*1;
% wq = 2*pi*30;

%% plots
% load('Td2.mat'); Td2p = Td2(2,:);
% load('thr.mat'); thrp = thr(2,:);
% load('th1.mat'); th1p = th1(2,:);
% load('hTd.mat'); hTdp = hTd(2,:);
% load('Td1.mat'); Td1p = Td1(2,:);
% load('th2.mat'); th2p = th2(2,:);



%% no disturbance
t = 0:1/1000:10;

load('no dist.mat');
figure;
plot(t,thrp,'--k','LineWidth',2); hold on
plot(t,th1p,'-.b','LineWidth',2); hold on
plot(t,th2p,'-r','LineWidth',2); hold off
grid on
legend('Reference','w/o DOB','proposed','location','southeast');
xlabel('Time (s)'); ylabel('Velocity (theta/s)');
xlim([0.5 60]);
```

```
%% disturbance 1
load('dist 1.mat');
figure;
plot(t,thrp,'--k','LineWidth',2); hold on
plot(t,th1p,'-.b','LineWidth',2); hold on
plot(t,th2p,'-r','LineWidth',2); hold off
grid on

legend('Reference','w/o DOB','proposed','location','southeast');
xlabel('Time (s)'); ylabel('Velocity (theta/s)');
xlim([0.5 60]);

figure;
plot(t,Td1p,'--m','LineWidth',2); hold on
plot(t,hTdp,'-g','LineWidth',2); hold off
grid on

legend('$T_d$','$\hat{T}_d$','interpreter','latex','location','southeast');
xlabel('Time (s)'); ylabel('Velocity (theta/s)');
xlim([2 60]);

%% disturbance 2
load('dist 2.mat');
figure;
plot(t,thrp,'--k','LineWidth',2); hold on
```

```
plot(t,th1p,'-.b','LineWidth',2); hold on
plot(t,th2p,'-r','LineWidth',2); hold off
grid on

legend('Reference','w/o DOB','proposed','location','southeast');
xlabel('Time (s)'); ylabel('Velocity (theta/s)');
xlim([0.5 60]);

figure;
plot(t,Td2p,'--m','LineWidth',2); hold on
plot(t,hTdp,'-g','LineWidth',2); hold off
grid on

legend('$T_d$','$\hat{T}_d$','interpreter','latex','location','southeast');
xlabel('Time (s)'); ylabel('Velocity (theta/s)');
xlim([2 60]);
```